



Assessment of Risks Induced by Countermining Unexploded Large-Charge Historical Ordnance in a Shallow Water Environment-Part I: Real Case Study

Nathalie Favretto-Cristini, Thierry Garlan, Olivier Morio, Xavier Demoulin,
M. Arrigoni, Anne Deschamps, Mickael Bonnin, Beucler É., D. Mercerat,
David Ambrois, et al.

► To cite this version:

Nathalie Favretto-Cristini, Thierry Garlan, Olivier Morio, Xavier Demoulin, M. Arrigoni, et al.. Assessment of Risks Induced by Countermining Unexploded Large-Charge Historical Ordnance in a Shallow Water Environment-Part I: Real Case Study. IEEE Journal of Oceanic Engineering, 2022, 47 (2), pp.350-373. 10.1109/JOE.2021.3111819 . hal-03598273

HAL Id: hal-03598273




<https://ensta-bretagne.hal.science/hal-03598273>

Submitted on 21 Apr 2022

HAL is a multi-disciplinary open access archive for the deposit and dissemination of scientific research documents, whether they are published or not. The documents may come from teaching and research institutions in France or abroad, or from public or private research centers.

L'archive ouverte pluridisciplinaire **HAL**, est destinée au dépôt et à la diffusion de documents scientifiques de niveau recherche, publiés ou non, émanant des établissements d'enseignement et de recherche français ou étrangers, des laboratoires publics ou privés.

Assessment of Risks Induced by Countermining Unexploded Large-Charge Historical Ordnance in a Shallow Water Environment—Part I: Real Case Study

Nathalie Favretto-Cristini , Thierry Garlan, Olivier Morio, Xavier Demoulin, Michel Arrigoni, Anne Deschamps, Mickaël Bonnin, Éric Beucler, E. Diego Mercerat , David Ambrois, Romain Schwab, Paul Cristini , *Member, IEEE*, and Fang Wang

Abstract—The goal of the work presented in a two-companion paper is to pave the way for reliably assessing the risks of damage to buildings on the shore, induced by the detonation of unexploded historical ordnance (UXO) of large weights in variable shallow water environments with a water depth less than 50 m. The risk assessment is quantified through the seismic magnitude on the Richter scale, induced by the detonation of charges of different weights (between 80- and 680-kg TNT-equivalent). This metric is investigated experimentally using a coupled seismo-acoustic approach within the framework of a UXO clearance (countermining) campaign in the Mediterranean Sea. Analysis of real acoustic and seismic data shows that, compared to a charge detonation in water, a similar detonation on the seabed generates seismic signals of lower frequencies and higher amplitudes that propagate in the seabed. The larger the charge weight, the higher the seismic amplitude. Besides the explosion-coast distance, the ground properties also

affect the signals. The sediments favor a longer signal duration and the presence of late dispersive and very low-frequency signals with a large amplitude, whereas the rocky grounds better preserve the high-frequency energy propagation. For the local environment considered in this study, a charge detonation on the seafloor generates seismic events of higher magnitudes compared to a detonation in water. However, these magnitudes are likely low enough to prevent any large damage in the nearby inland infrastructures.

Index Terms—Charge weight/seismic magnitude relationship, seismic risks, seismo-acoustic signals, underwater explosion.

I. INTRODUCTION

UNEXPLODED historical ordnance (UXO) from World War II (WWII) is still discovered almost every week close to the French coasts (OSPAR Commission Report found at <https://www.ospar.org/work-areas/eiha/munitions>). Quickly after their discovery, the French Navy Mine Warfare Office (FNMWO) must destroy the munitions, to ensure the safety of divers and ships. The favored destruction method is countermining, i.e., to use a high-order detonation conducted by exploding an additional donor charge placed adjacent to the UXO munition [1]. Depending on whether the UXO is safe to move, such countermining occurs at specific safe locations or at the location of the discovery. The risks for people in charge of the UXO countermining are well known by the Mine Warfare experts.

In contrast, the possible consequences of underwater explosions on the marine environment (e.g., small landslides) and on the buildings located on the coast (e.g., structural damages, window breaking) are more difficult to control because they are much more complex to reliably evaluate. Indeed, they depend mostly on the environment geology and the characteristics (weight and location) of the explosive charges, and hence on the shock-induced wave propagation. However, it would be useful to rely on (at least) one reliable metric that would help develop a decision support tool for the risk assessment regarding inland infrastructures.

To define this metric, we propose to take advantage of the fact that the UXO countermining is generally recorded at the regional scale by the permanent seismic networks. A seismic magnitude on the Richter scale can therefore be calculated for each explosion, as it is done for natural (i.e., tectonic) sources [2]. We then

Manuscript received October 9, 2020; revised June 8, 2021; accepted September 5, 2021. This work was supported by The French National Research Agency (ANR) and cofunded by DGA (French Ministry of Defense Procurement Agency) under Reference Project ANR-15-ASTR-0001 POSA. (Corresponding author: Nathalie Favretto-Cristini.)

Associate Editor: N. R. Chapman.

Nathalie Favretto-Cristini and Paul Cristini are with Aix-Marseille University, CNRS, Centrale Marseille, LMA, 13013 Marseille, France (e-mail: favretto@lma.cnrs-mrs.fr; cristini@lma.cnrs-mrs.fr).

Thierry Garlan and Olivier Morio are with Shom/DOPS/STM/SEDIM, Marine Geology Department, Service hydrographique et océanographique de la Marine, 29228 Brest, France (e-mail: thierry.garlan@shom.fr; olivier.morio@shom.fr).

Xavier Demoulin is with MAREE, Parc Technologique de Soye, 56270 Ploemeur, France (e-mail: xdemoulin@maree.fr).

Michel Arrigoni is with ENSTA Bretagne, Institut de Recherche Dupuy de Lôme, CNRS UMR 6027, 29806 Brest, France (e-mail: michel.arrigoni@ensta-bretagne.fr).

Anne Deschamps and David Ambrois are with Université Côte d'Azur, CNRS, IRD, Observatoire de la Côte d'Azur, Géoazur 06560 Sophia Antipolis, France (e-mail: anne.deschamps@univ-cotedazur.fr; david.ambrois@gmail.com).

Mickaël Bonnin and Éric Beucler are with the LPG—Université de Nantes, Université d'Angers, CNRS UMR 6112, 44322 Nantes, France (e-mail: mickael.bonnin@univ-nantes.fr; eric.beucler@univ-nantes.fr).

E. Diego Mercerat is with Equipe Repsody, CEREMA Méditerranée, 06903 Sophia Antipolis, France (e-mail: diego.mercerat@cerema.fr).

Romain Schwab was with the MAREE, Parc Technologique de Soye, 56270 Ploemeur, France. He is now with ENSTA Bretagne, Lab-STICC, 29238 Brest, France (e-mail: romain.schwab@ensta-bretagne.fr).

Fang Wang was with the Aix-Marseille University, CNRS, Centrale Marseille, LMA, 13013 Marseille, France. She is now with CGG, 91300 Massy, France (e-mail: alinewf.wang@gmail.com).

Digital Object Identifier 10.1109/JOE.2021.3111819

suggest to assess the seismic risk through the seismic magnitude induced by the underwater explosion. As a result, the relationship between the charge (UXO) weight and the seismic magnitude induced by the underwater explosion has to be known.

In seismology, the magnitude of a regional seismic event is classically derived from the signals recorded at numerous permanent seismic stations that are located far from the source (i.e., in the far field, usually at distances between 30 and 500 km), to average the influence of the medium heterogeneities along the propagation paths. The underlying idea is to derive a robust metric that is as much free of “site effects” as possible.

Unfortunately, as the UXO countermining usually takes place at close distances from the shoreline, the geological environment (e.g., the sedimentary basins) can have a significant imprint on the seismic signals that reach the inland infrastructures. As a result, in the perspective of developing a decision support tool, it is relevant to determine how significant the site effects are, and to what extent these “near-field” effects may impact indirectly the final outcome of the seismic magnitude derived for “far-field” conditions. In other words, it is necessary to investigate whether we can rely on the seismic magnitudes derived only from permanent seismic networks located in the far field of the explosions to assess what happens in the near-field of the large underwater explosions.

As a consequence, relying on the seismic magnitude for risk assessment requires a proper understanding of the relationship between the charge weight, the propagation of the explosion-induced waves, and the marine environment beforehand. In other words, we have to understand how the seabed and the water layer influence the propagation of the seismo-acoustic waves that are generated by the UXO detonation and that reach the coast. In this article (Part I), we investigate this influence experimentally, whereas in Part II [3], we will rely on numerical simulations.

The relationship between the charge weight and the seismic magnitude induced by the underwater explosion is poorly addressed in the literature, except in specific works dedicated to forensic seismology that helps verify compliance with the Comprehensive-Nuclear-Test-Ban Treaty [4], [5], or that helps identify the causes of dramatic incidents, like unexpected ship sinking [6], [7].

The relationship between the charge weight and the marine environment, through the wave propagation, is usually studied for the case of relatively small charges (generally, smaller than a few-kilograms TNT-equivalent weight) and/or relatively deep seabeds (e.g., [8]–[10]). To the best of our knowledge, very few works are concerned with charges of a few-hundred-kilograms TNT-equivalent weight [11], [12] and located in coastal waters with a depth less than 50 m [13]–[15]. However, the UXO of WWII usually satisfies these conditions, in particular along the French coasts of Brittany and the Mediterranean Sea. Consequently, there is a strong need for a better understanding of the relationship between the wave propagation generated by the explosion of large charges and the properties of the very shallow water environment, for a reliable risk assessment with respect to inland infrastructures.

Nevertheless, the interdisciplinary nature of this problem makes it incredibly challenging. Indeed, defining this relationship implies to 1) evaluate/measure the mechanical response produced by the detonation of various large charges in very shallow waters; 2) understand the effect of the physical and geometrical characteristics of the coastal environment (that are often variable along the wave path in shallow waters) on the seismo-acoustic wave propagation generated by the explosion; and 3) estimate the seismic response that could be recorded at an observation point on the land coast.

Thanks to an abundant literature in several disciplinary fields (e.g., detonics, underwater acoustics, marine seismics, mechanics), the physical process of underwater explosions is now well identified (e.g., [16]–[19]), and the general characteristics of the explosion-induced signal, composed of the signals associated with the shock wave and the bubble oscillation pulses, are well established. The characteristics, such as waveform, spectrum, energy level, peak pressure, have been determined for small charges (generally, of TNT-equivalent weights from a few hundred grams up to a few tens of kilograms at most) through direct measurements by hydrophones or ocean-bottom seismometers (OBS) (e.g., [20]–[25]), or by means of inversion process [7]. It has to be pointed out here that an inversion process may be much more complicated in coastal zones since the wave travel paths are complex and the resulting signals are affected by interferences between the reflections from the water surface and the sea bottom, and thus its geological nature. Also, note that the characteristics of the explosion-induced signal may be slightly different according to the UXO location compared to the sea bottom [25]. Despite this abundant literature, works that are focused on the characteristics of charges of hundred kilograms TNT-equivalent weights and located in shallow water environments, except those reported in [13]–[15] and [26], are still lacking. This can be explained by the fact that the recording systems such as hydrophones or OBS, deployed in the near-field of the explosion, can be damaged.

Since they provide a pulse source of great power and of broad frequency range, the explosive charges have been traditionally used as sources for marine seismic surveys, before the advent of the sources of airgun type, with the ultimate goal of retrieving the properties of the deep bottom layers (e.g., [21] and [13]). The explosive charges are also used in underwater acoustics for studying the propagation of interface waves of the Stoneley–Scholte type and for evaluating the shear wave properties of the first meters of the sedimentary layers (e.g., [27] and [28]). However, the charges are often of small TNT-equivalent weights, and the detonation-induced shock propagation occurs in quite academic configurations where the sediments and the water layer have a relatively constant thickness (e.g., [10], [28], and [29]).

Moreover, to the best of our knowledge, there are very few works that couple both the acoustic and the seismic wave propagation in the coastal zones where the depth of the water layer and the thickness of the sedimentary layer are variable. Nevertheless, accounting for this coupling is essential when the low-frequency (LF) propagation is involved in shallow water configurations because the presence of the sedimentary basins may have a

great influence on the wave propagation, as is well known in seismology (e.g., [9] and [30]–[33]).

One of the main goals of our work, presented here in a two-companion article, is to pave the way for assessing the seismic risks, induced by the underwater detonation of large-charge historical ordnance in variable shallow water environments, to which buildings and infrastructures on the shore may be exposed. “Large charge” here means charges of up to 680-kg TNT-equivalent weights, and “shallow water” means a water depth less than 50 m, which corresponds to a different configuration compared to those considered in previous works reported in the literature.

As mentioned earlier in the Introduction, the relationship between the large charge weight and the seismic magnitude, induced by the underwater explosion and recorded on the land coast, has to be understood and evaluated in a reliable manner. This implies to estimate the acoustic response of the explosion according to the charge weight. This also implies to study the impact of the variability in the (acoustical and geometrical) properties of the very shallow marine environment, including the impact of the properties of the sedimentary layer, on the seismo-acoustic wave propagation from the explosion to the coast. To achieve this goal, we rely on a multidisciplinary cross-study between a real case study and numerical modeling.

In the framework of a countermining campaign, called the POSA project, and conducted in December 2018 in the Rade d’Hyères (France), in the Mediterranean Sea, acoustic and seismic recording systems have been deployed to record the explosion-induced waves in the water and the seismic signals on the land coast. These acoustic and seismic measurements, coupled to information provided by geological surveys, enable the questions of interest to be partially answered through the real data analysis.

However, a deeper interpretation of the real data is needed, and a better understanding of the physics of the seismo-acoustic wave propagation in a variable shallow marine environment could help. Therefore, a numerical modeling of the realistic seismo-acoustic propagation was developed using the *in situ* acoustic and geological measurements as input data. The cross-validation between the numerical simulations and the real seismic data sheds light on the key parameters with the associated uncertainties and limitations that really impact the wave propagation. This feedback is very useful for future development of a decision support tool for the assessment of seismic risks, induced by underwater explosions, for inland infrastructures. Part II of the paper [3] describes the numerical modeling of the explosion-induced seismo-acoustic wave propagation in the Rade d’Hyères (France) and the results of the cross-validation between the numerical simulations and the real seismic data.

Part I, of interest here, is focused on the real case study of the risks induced by countermining unexploded large-charge ordnances in a very shallow water environment, namely the Rade d’Hyères (France), in the Mediterranean Sea. The goal of this article is twofold: 1) analyze the acoustic and seismic data recorded during the countermining of different large explosive charges (from 80- up to 680-kg TNT-equivalent weights), and

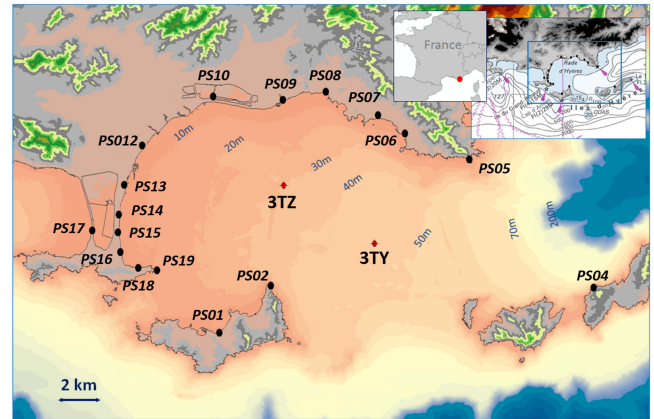


Fig. 1. Experiment site (Rade d’Hyères, France), the two locations (3TY and 3TZ) where the UXO was detonated during the campaign of December 2018, and the location of the 17 sites where temporary seismological stations have been deployed along the land coast. The bathymetry is indicated by the color scale.

draw preliminary conclusions regarding the risk assessment with respect to inland infrastructures; and 2) provide the input data (i.e., geologic and acoustic data) and the output data (i.e., seismic data) for the numerical modeling and the cross-validation tasks developed in [3].

First, Section II presents the experiment location and its geomorphology determined from geological and acoustical measurements. The conditions of the countermining of the explosive charges of various weights, as well as the acoustic and seismic recording systems deployed in the water column and along the shore, are then described in Section III. Section IV presents the acoustic data, and focuses on the contribution of the shock wave and the first bubble pulse, generated by the detonation of the different charges, on the acoustic field in water. Section V presents the explosion-induced seismic data and investigates the effect of both the environment and the detonation conditions on the seismic data. Section VI focuses on the derivation of the relationships between the charge weights and the explosion-induced seismic magnitudes. These relationships enable to draw preliminary conclusions on the risk assessment with respect to inland infrastructures. Finally, the article ends with still open questions that are addressed subsequently in [3], thanks to the additional numerical modeling and analysis reported there.

II. LOCATION OF THE EXPERIMENT SITE AND ITS GEOMORPHOLOGY

In December 2018 we conducted a unique seismo-acoustic experiment involving large-charge UXO in the Rade d’Hyères (south-eastern part of France; see Fig. 1), thanks to a fruitful cooperation with the FNMWO. The purposes of this joint experiment (included in the POSA project) were twofold: for the FNMWO, to destroy safely UXO, and for us, to record acoustic and seismic explosion-induced signals in the coastal water and on the land coast. The POSA project aimed to study the seismo-acoustic wave propagation generated by the

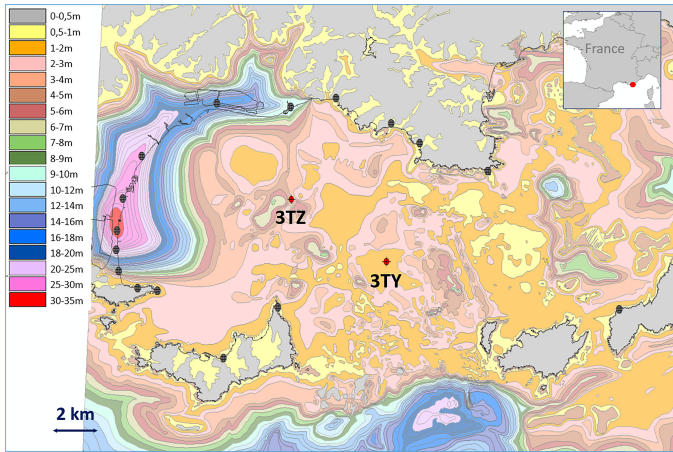


Fig. 2. Detailed 3-D map of the thickness of the sedimentary layer in the Rade d'Hyères and in its vicinity.

countermining of UXO of large weights in shallow waters, and the possible consequences on the buildings located on the land coast.

The explosive charges were detonated at two specific locations in the bay (labeled 3TY and 3TZ, respectively, in Fig. 1). The source distance from the land coast ranges from 6 to 13 km. The bathymetric map of the Rade d'Hyères shows that the water depth at the experiment site varies within the 0–50-m range (see Fig. 1). At the locations 3TY and 3TZ, the water depth was 46 and 29 m, respectively, with an uncertainty of ± 0.5 m.

Before the countermining campaign, acoustic and geological surveys were conducted to get information on the seabed geomorphology and on the water column. Particular attention was paid to the characteristics of the sediments.

High-resolution sub-bottom profiling surveys [34] provided a detailed 3-D map of the thickness of the sedimentary layer, evaluated every 20 m along a horizontal spatial grid with a thickness uncertainty of ± 1 –2 m (see Fig. 2). Globally, the sediment thickness is small (including at the explosion locations) and varies within the 1–5-m range. However, there is a sedimentary basin, close to the western part of the land coast, whose thickness ranges from 15 to 30 m. Based on these new acoustic measurements, on the analysis of the new core samples, and on archival results from previous core samples (e.g., [35] and [36]), the seabed has been globally described as sandy sediments with a fine grain size, except locally and close to the western part of the land coast where there is a mixture of fine sands and muds (see Fig. 3).

The nature of the bedrock underlying the sedimentary layer was mainly extrapolated from geological outcrops or from measurements performed on pieces of rocks present in the sedimentary core samples. It is mainly composed of Sauvette's phyllades (that are weakly metamorphic schists rich in sericite and chlorite and alternating with quartz beds), except close to the western part of the land coast where there is Sauvette's mica schist. Locally, thin corridors of gneiss with tourmaline and quartzite are stretched from the northern to the southern part of the Rade (see Fig. 3).

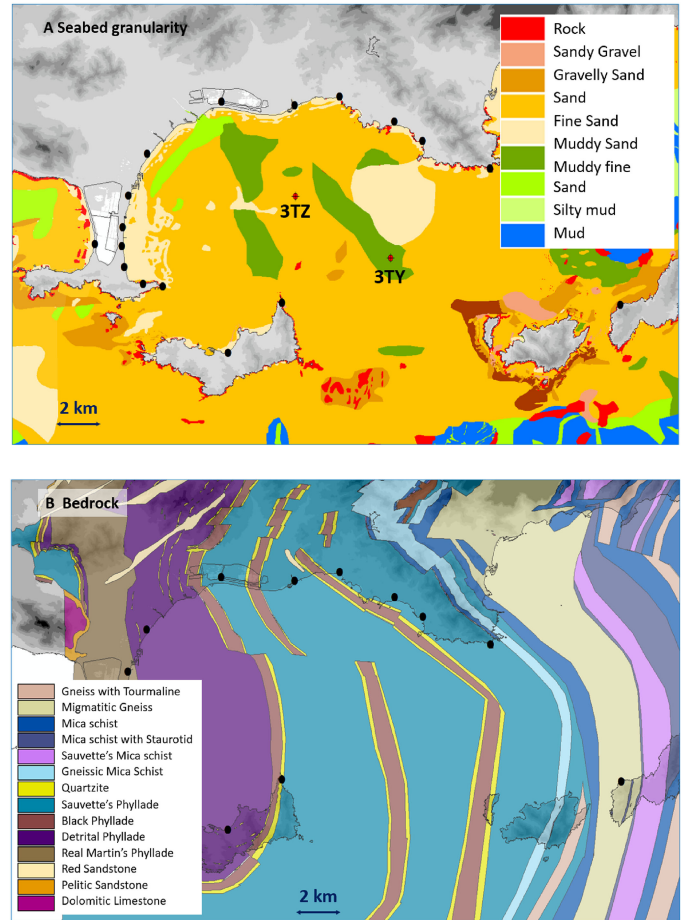


Fig. 3. Three-dimensional geological and geomorphological model of the Rade d'Hyères and its vicinity: focus on the nature of the sediments and the rocky basement.

Note that no specific survey was conducted to get information on the sound-speed profile in the Rade d'Hyères. From a single measurement of the water temperature, and taking into account the salinity of the Mediterranean Sea, the sound speed was assumed constant within the Rade d'Hyères and equal to 1507 m/s.

III. HYDRO-ACOUSTIC AND SEISMIC EXPERIMENTS

During the experiment, a series of eight underwater explosions generated by the countermining of eight cylindrical explosive charges of TNT-equivalent weights ranging from 80 to 680 kg were detonated. The largest charges consisted of bundles of smaller cylindrical charges (namely, charges of 80-kg TNT-equivalent filled with TRITONAL 80/20, and charges of 200-kg TNT-equivalent filled with HBX-3) stacked together in a container [see Fig. 4(a)]. All the explosive (TRITONAL 80/20 or HBX-3) weights have been converted into TNT-equivalent weights by applying a TNT-equivalent ratio of 1.2. This ratio, provided by the French Navy, is consistent with the ratios indicated in [37], considering the fact that a TNT-equivalent ratio for underwater conditions is higher than for air conditions, as suggested in [38]. However, due to uncertainties on the TNT



Fig. 4. (a) Charges of 200-kg (left) and 80-kg (right) TNT-equivalent stacked in a container, before being dipped to water. (b) Ship named *BSAD Ailette* that transported the charges to the locations of their countermining.

equivalency for the given explosives, a $\pm 10\%$ uncertainty factor is to be considered on the weight of the TNT-equivalent charges.

The ship named *BSAD Ailette* [see Fig. 4(b)] transported the explosive charges to the two specific locations labeled 3TY and 3TZ, respectively, in Fig. 1. A crane was then used for dipping the charges to the water.

Ground-truth information, including the estimated location of the charges, the charge weight, the shot depth, the water depth, and the local time of the detonations, is presented in Table I. Although the coordinates were measured by a precise differential GPS system, we could not estimate the actual location with an accuracy better than 10–15 m because the ship was in motion when the explosives were dropped. Moreover, the local time of the detonations could not be measured with an accuracy better than 1 s because of the imprecise dating of the recording files. Note that the first seven (S1–S7) charges were placed on the sea bottom, whereas the last one (S8) was placed in a container in the water column. The latter configuration thus allowed a direct comparison between the seismic explosion-induced effects on the land coast when explosions (generated by charges of same weights) occur at the sea bottom or in the water column.

As the published works concerned with the detonation of large explosive charges in shallow waters are sparse, we collected acoustic data to gain insight on the source signal. These acoustic

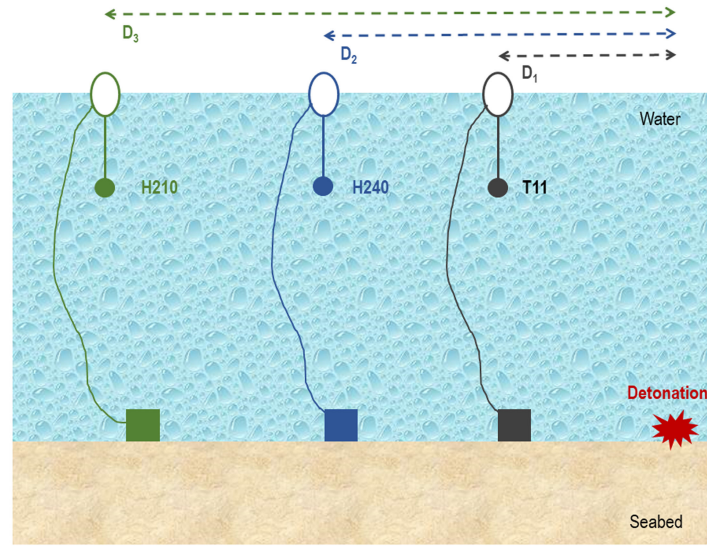
data were collected by means of a hydro-acoustic recording system (see Fig. 5), consisting of a shock-gauge transducer and two hydrophones. The shock-gauge transducer was placed at a water depth of $10 \text{ m} \pm 1 \text{ m}$ from the sea surface, and at fairly close horizontal distances (from 110 to $270 \text{ m} \pm 5 \text{ m}$; see Table I) from the explosive charge locations, for subsequently estimating the source (explosion) signature. The two hydrophones were suspended from a small buoy at a water depth of 10 m and at distances equal to $D_2 \sim 400 \text{ m}$ and $D_3 \sim 3000 \text{ m}$ (during the first experiment day), and $D_2 \sim 2800 \text{ m}$ and $D_3 \sim 5900 \text{ m}$ (during the second experiment day), from the shot locations (see Table I). They were used to subsequently estimate the explosion-induced wave propagation in the water column.

The shock-gauge transducer T11 (manufactured by Neptune Sonar) had a nominal charge sensitivity of 0.07 pC/kPa and could record pressures up to 275 MPa, with a rise time of less than $4 \mu\text{s}$. Unfortunately, the bandwidth of the transducer is not accurately known. The transducer was powered by a Müller charge amplifier-system MCPA 10. A four-channel RT-SYS SDA14 data recorder was used to capture the data. The SDA14 device had a -3-dB/octave highpass filter at 5 Hz, and a 15-dB input gain was applied. The shock-transducer signals were recorded continuously, and the signal digitization occurred at a sampling rate of 625 kHz, giving a time resolution of $1.6 \mu\text{s}$. As the maximum pressure level that was recorded during the

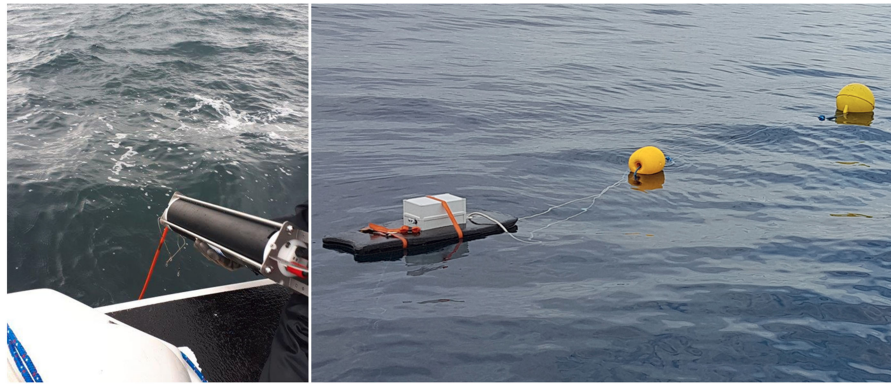
TABLE I
GROUND-TRUTH INFORMATION CONCERNING THE EIGHT EXPLOSIONS GENERATED BY THE COUNTERMINING OF THE EIGHT CHARGES

Explo. (sources)	Charge location	Charge TNT-eq. weight (kg)	Shot depth (m)	Water depth (m)	Range D_1 (m) - Transd. T11	Range D_2 (m) - Hydro H240	Range D_3 (m) - Hydro H210	Local time
S1	3TZ	80 ± 8	29 ± 0.5	29	160 ± 5	408	2 957	13:13:29
S2					122 ± 5	391	3 076	14:03:02
S3	3TY	80 ± 8	46 ± 0.5	46	110 ± 5	326	2 983	15:28:20
S4		680 ± 68			272 ± 5	2 878	5 939	07:20:28
S5		600 ± 60			245 ± 5	2 841	5 903	08:10:43
S6		400 ± 40			257 ± 5	2 848	5 909	09:03:18
S7		200 ± 20			239 ± 5	2 837	5 898	09:48:34
S8		80 ± 8	11 ± 0.5		269 ± 5	2 844	5 906	12:37:49

The shots S1 to S3 and the shots S4 to S8 were performed on December 11–12, 2018, respectively.



(a)



(b)

Fig. 5. (a) Hydro-acoustic recording system, consisting of a shock-gauge transducer (T11) and two hydrophones (H210 and H240), deployed in the water column to estimate the explosion parameters. (b) RTSYS SDA14 autonomous recorder deployed for the hydrophones (H210 and H240) recordings. (c) Shock-gauge transducer (T11) attached by a rubber band to a bodysurf carrying the electronics. Such a design is effective in preventing shock wave damage.

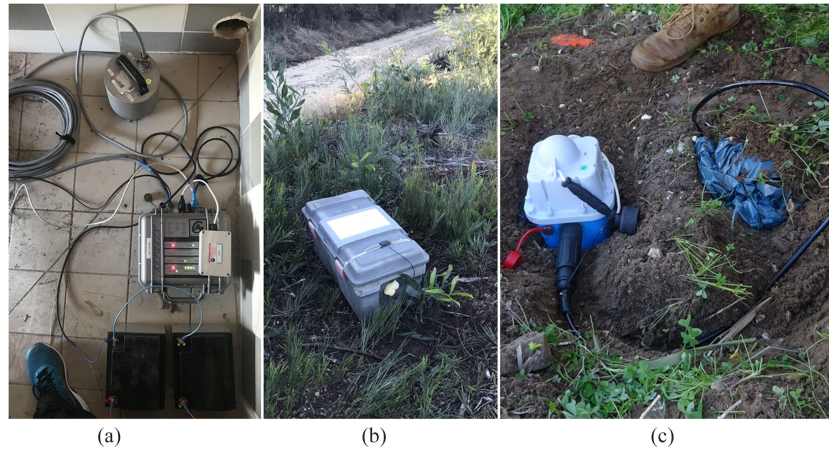


Fig. 6. (a) Broadband sensor and a digitizer installed in a small room at the location labeled PS12 in Fig. 1. (b) and (c) When the instruments were installed outside, the sensors were buried, and all the associated parts (digitizer, disk, and batteries) were placed in a plastic box, as illustrated (b) for the sensor located at PS07 in Fig. 1.

experiments was around 1 MPa (see Fig. 8), i.e., well below the limit of the measurement system, there was no clipping.

The two hydrophones were Hi-Tech model HTI-96 with nominal sensitivities of -210 dB re 1 V/ μ Pa (hereafter, referred to hydrophone H210) and -240 dB re 1 V/ μ Pa (hereafter, referred to hydrophone H240), respectively. They had flat responses (within 3 dB) over the frequency band 2–30 000 Hz. A four-channel RTSYS SDA14 data recorder was used to capture the data. The SDA14 device had a -3 -dB/octave highpass filter at 5 Hz, and a 15-dB input gain was applied by default. The hydrophone signals were recorded continuously, and the signal digitization occurred at a sampling rate of 78.125 kHz, giving a time resolution of 12.8 μ s. The limit of the measurement system was finally 6.68 kPa for the hydrophone H210 and 214.5 kPa for the hydrophone H240. Due to its rather insensitive nature, the hydrophone H240 could make unclipped recordings of all the explosions (even for the largest ones). Unfortunately, clipping could not be avoided for the most energetic part of the signals recorded by the hydrophone H210, despite the fact that the mooring was removed as far as possible from the explosion area.

As the main goal of our work was to assess the seismic risks induced by large explosions, it was essential to collect seismic data on the land coast that could help study the variation of the ground response as a function of the explosive charge weights, and as a function of the properties of the marine environment. As a consequence, a temporary seismic network consisting of 20 three-component broadband velocimeters and accelerometers (see Fig. 6) was deployed all along the land coast on 17 sites at distances ranging from 6 to 13 km from the explosion locations (see Fig. 1, and Table II in Appendix 1). The seismological stations recorded continuously during their installation period, including the seismic ground motion generated by explosions. The seismic signals were recorded with sampling rates of 250 samples per second (sps) (velocimeters) and 500 sps (accelerometers), respectively. For the purpose of data analysis, the signals associated to each source were provided as 4-min-long three-components records in three different forms, namely raw data associated with metadata describing the instrumental response, ground velocities, and ground accelerations. The

corrected data were then bandpass filtered, between 0.1 and 45 Hz for 250-sps signals, and between 0.1 and 110 Hz for 500-sps signals.

IV. ACOUSTIC EXPLOSION-INDUCED SIGNALS

As already mentioned in the Introduction, the published works concerned with the detonation of large explosive charges in shallow waters are sparse. As a result, any new investigation of acoustic detonation-induced signals is of interest to gain insight into the effect of the charge characteristics and into the effect of propagation. This is the purpose of this section.

We first analyze the acoustic signals recorded by the shock transducer at a single position to compare the impact of the different charge weights. We then study the acoustic signals recorded by the hydrophones located at two different positions from the source to study the effect of propagation paths. The impact of the location of the source, namely on the seabed or in the water column, is also investigated. Some of these results will provide the input data for the numerical modeling developed in [3].

A. Signals Recorded by the Shock Gauge Transducer

Time-series data for the explosion S3 (corresponding to a charge of 80-kg TNT-equivalent; see Table I), recorded by the shock gauge transducer T11 located at the distance of 110 m from the source, are shown at different time scales in Fig. 7.

The signal associated with the shock wave highlights the typical feature of a shock waveform, namely an instantaneous pressure rise (with a peak pressure at 0.15 s) followed by an exponential pressure decay [see Fig. 7(c)]. This arrival time considers the pyrotechnic delay from the surface and the detonating cord that ignites the explosive charge. Thus, it cannot be considered as a reliable arrival time of the shock wave after detonation.

Indeed, it is important to mention here that it is extremely difficult to perfectly synchronize the triggering of the acquisition system with the exact moment of the underwater explosion. The firing was ignited at the sea surface on a booster charge that

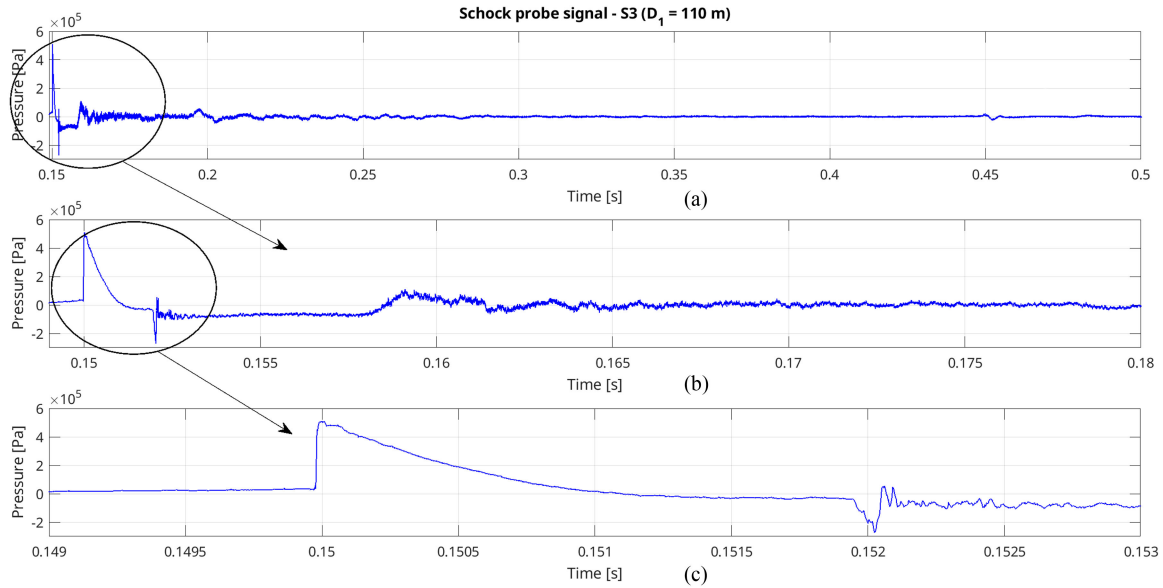


Fig. 7. Signal generated by the explosion S3 (corresponding to an 80-kg TNT-equivalent charge) and recorded by the shock gauge transducer T11. Different time scales allow to clearly observe the shock wave arrival at ~ 0.15 s and the bubble pulse arrival at ~ 0.45 s. The signal arriving at ~ 0.152 s is associated with waves reflected by the free surface.

detonated a detonating cord going 10 m down to the sea surface around the main charge. As the Chapman–Jouguet velocity of the detonating cord is about 3000 m/s, it thus took about 3 ms for the detonation to run the distance from the detonator to the main charge. Therefore, we estimate that there is a delay of at least 0.09 s between the trigger and the instant of detonation that is mainly due to the firing chain (firing switch, detonator, detonating cord). As a result, we consider that the arrival time of the shock wave is less meaningful than the arrival time difference between the shock wave and the subsequent bubble pulses.

Considering the expressions for the maximum bubble radius and the vertical migration given in [39], the charges were deep enough to generate at least the first bubble pulse, whatever the charge weight, and wherever the location of the explosion (i.e., either on the seabed at a water depth of 29 or 46 m, or in the water column at a depth of 11 m). The first bubble pulse can be seen arriving ~ 0.30 s after the primary shock arrival [see Fig. 7(a)], which is consistent with empirical predictions [8], [22]. The signal arriving at ~ 0.152 s [see Fig. 7(b) and (c)] is associated with the waves reflected by the free sea surface and received before the completion of the bubble pulse from the direct wave.

It is worth noting here that the difference of 2 ms in the arrival times between the direct and the first surface reflected paths corresponds to a distance variation of 3 m. This condition may be fulfilled if the T11 sensor was actually located at 4 m below the sea surface (instead of 10 m) and closer to the source (at the horizontal distance $D_1 \sim 101$ m, instead of 110 m). This may be consistent with the hypothesis that the sensor could have been pulled horizontally to a shallower depth by the water stream induced by the wind. However, the condition of the distance variation of 3 m may be also fulfilled if a cavitation surface was

present below the sea surface. Indeed, as the cavitation surface acts as a free surface, the direct wave from the source could have been reflected by this bubbly surface, instead of the sea surface, before reaching the T11 sensor. The time difference remains unexplained because we cannot revisit the experimental conditions for further tests.

The signal associated with the shock wave generated by the explosions on the seabed has the same waveform, whatever the TNT-equivalent charge weight (see Fig. 8). However, the shock waveform is very different for the case of an explosive charge located in a container in the water column, which is consistent with the results reported in the literature (see, e.g., [40, Figs. 8 and 10]). In particular, the exponential pressure decay following the pressure rise is largely missing because its positive phase duration is much longer than the time taken by the wave reflected from the free surface to reach the sensor, causing a so-called “cutoff” (i.e., a fast pressure drop). In addition, for the largest charges (for instance, for the explosion S6 corresponding to a charge of 400-kg TNT-equivalent), the exponential pressure decay may exhibit a peak, observed 1 ms after the first peak corresponding to the arrival of the shock wave. As the charge consisted of two charges of 200 kg attached together, it is likely that the time difference corresponds either to a pyrotechnic delay, or to a difference of almost 1 m between the center of the two explosives. In any case, this demonstrates the complexity in composite detonations.

It is also important to mention that, since the sampling frequency of the DAQ system for the shock transducer is 625 kHz, the rising front of the shock wave contains only three samples, which makes challenging the measurement of the maximal overpressure. However, Fig. 9 shows the measured maximal sound pressure from the underwater explosions, together with the associated uncertainties, as a function of the charge weight

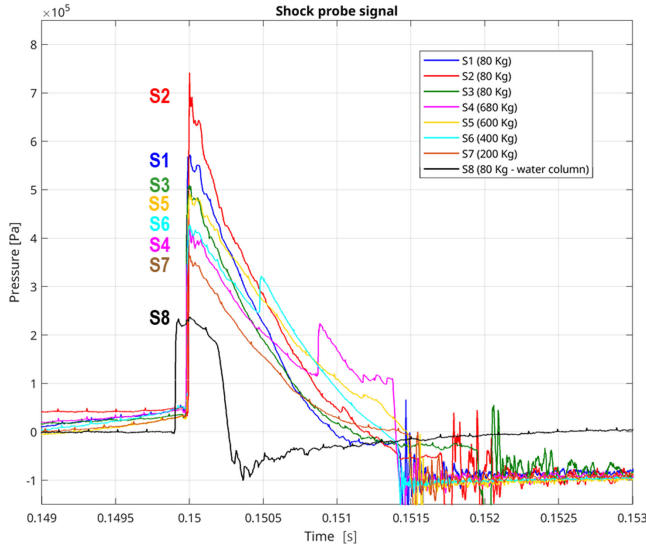


Fig. 8. Focus on the first 4 ms of the signals generated by the explosions S1–S8 (corresponding to different charge weights and different charge locations, namely on the seabed and in the water column; see Table I) and recorded by the shock gauge transducer T11 located between 110 and 270 m from the sources. Note that, for illustrative purposes, the waveforms have been artificially superimposed, and that the amplitudes are not proportional to the charge weights, since the distance between each explosion location and the shock gauge transducer is different (effect of propagation).

W and as a function of the scaled range $R/W^{1/3}$, where R is the distance from the explosion.

Uncertainties on the scaled range are due to the misestimation of $\pm 10\%$ of the TNT equivalency of the charge and to the charge positioning error of ± 5 m, whereas uncertainties on the maximal peak pressure of $\pm 5\%$ are due to the sensor sensitivity and to the digitizer resolution. It is also observed that the pressure data measured at close distances from the charge are more likely subjected to higher uncertainties, which is observed in air experiments as well, since the pressure rate is higher and thus more difficult to estimate.

From Fig. 9, we see that the peak pressure decreases with increasing scaled distance and with increasing immersion depth of the detonation.

Moreover, wherever they were acquired (site 3TZ or 3TY), our measurements do not fit the curve for the peak pressure P_{peak} (in MPa) given by the empirical law reported in the literature (e.g., [8] and [10]) and that applies for shallow charges in deep water

$$P_{\text{peak}} = 52.4 \left(R/W^{1/3} \right)^{-1.13} \quad (1)$$

where R is the distance (in m) from the explosion, and W is the charge weight (in kg TNT-equivalent). Instead, for instance, for the site 3TY where the water depth was 46 m, our measurements rather follow the curve resulting from the power law fit

$$P_{\text{peak}} = 9.159 \left(R/W^{1/3} \right)^{-0.873} \quad (2)$$

Equation (2) greatly differs from (1). In contrast to the empirical law that is defined for an “open” (deep water) environment,

(2) implicitly accounts for the environment characteristics (essentially, the bathymetry and the impedance contrast between water and the seabed). Equation (2) is related to the site 3TY, but not to the site 3TZ, as shown by the two values for the peak pressure that are well above the curve. Moreover, it seems that the location of the detonation (namely, on the seabed or close to the sea surface) does not strongly affect the peak pressure.

Since our dataset is sparse, additional experiments that could confirm the trends observed in Fig. 9 would be of valuable interest.

B. Signals Recorded by the Hydrophones

An illustration of the time-series data for the explosion S3 (corresponding to a charge of 80-kg TNT-equivalent; see Table I), and recorded by the two hydrophones H240 and H210 deployed at the distance of 326 and 2983 m, respectively, is provided in Fig. 10. Note that the signal recorded by the hydrophone H210, in particular the part of the signal with the highest amplitude (namely, the beginning of the shock wave signal), is slightly clipped.

The signal associated with the shock wave arrives at ~ 0.15 s. As mentioned before, since this time considers a pyrotechnic delay in addition to a triggering delay, it cannot be considered as the real arrival time. However, it is a valuable temporal mark to evaluate the transit time from one sensor to another for the same shot.

The first bubble pulse arrives ~ 0.30 s after this primary shock arrival on the two signals recorded by the two hydrophones. According to the Willis formula [41], the pulsation period T_b of the bubble in free water conditions should match the relationship

$$T_b = K_b W^{1/3} (H + 10)^{-5/6} \quad (3)$$

where K_b is a constant (in seconds) equal to 2.1 for TNT explosives and to 2.6 for HBX-3 or RDX explosives [42], H is the water depth (in meters), and W is still the charge weight (in kilograms TNT-equivalent). For a charge of 80-kg TNT-equivalent detonated at the 3TY location where the water depth is 46 m, this would lead to a pulsation period of about 316 ms. This theoretical pulsation period is then greater than the pulsation period we observed in our experiments (namely, ~ 0.30 s). At first sight, this seems inconsistent with the conclusions reported in [25], namely the presence of a seabed close to the explosion tends to increase the first bubble pulse period. However, from (3), we note that a misvaluation of the actual charge weight or a misestimation of the actual water depth may affect the theoretical period. It is also sensitive to the constant K_b considered for TNT [43]. These uncertainties may actually lead to an overestimation of the theoretical bubble pulse period.

In Fig. 10, we also observe that the longer range signal recorded by the hydrophone H210 is much more complex than the shorter range signal received at the hydrophone H240. Indeed, the longer range signal exhibits more effects of the shallow water environment on the wave propagation, mainly waveguide dispersion, and in a lesser extent reverberation effect as well.

For the sake of brevity of this article, we choose not to present all the signals recorded by the hydrophones, since the signals

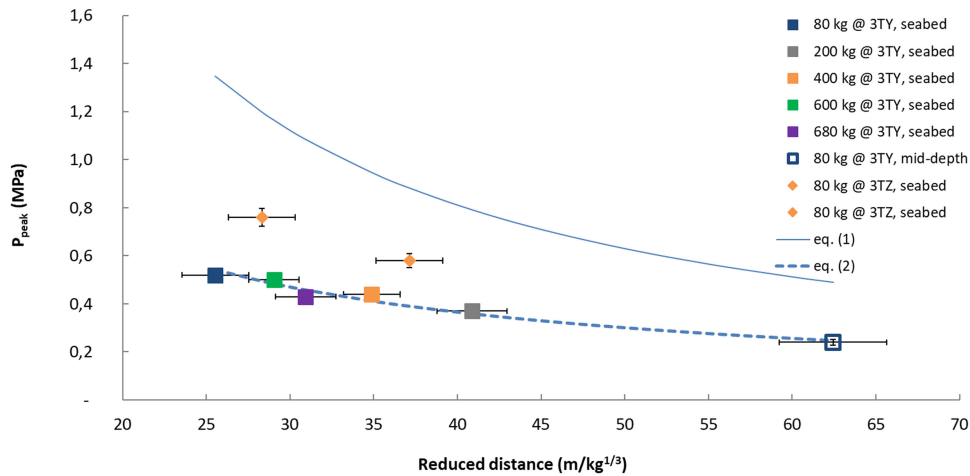


Fig. 9. Variation of the maximal overpressure recorded by the shock-gauge transducer T11 as a function of the scaled range for various explosive charges, detonated on the seabed or in the water column, at the different sites (3TZ and 3TY).

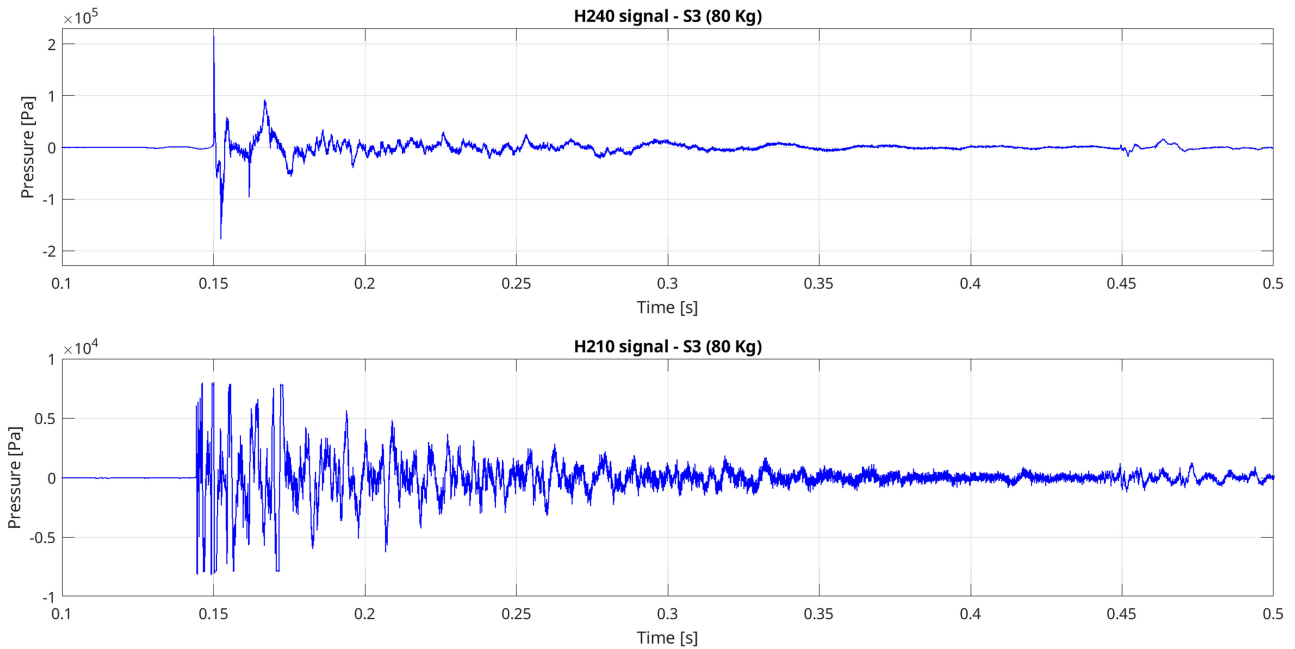


Fig. 10. Signals generated by the explosion S3 (corresponding to a 80-kg TNT-equivalent charge) located on the seabed at the location 3TY and recorded by the two hydrophones H240 (top) and H210 (bottom) located at 326 and 2983 m, respectively, from the source. For a better comparison, both signals are blocked on the same arrival time for the shock wave. Note that the part of the signal arriving at ~ 0.15 – 0.17 s and recorded by the hydrophone H210 is clipped.

have similar waveforms for similar detonation conditions, i.e., for similar charge weights and for similar shallow water environments. Nevertheless, the signal waveforms depend on the charge location at a same experiment site, as it is illustrated in Fig. 11. More specifically, the signals associated with the bubble pulse have globally higher amplitudes when the charge is located in a container in the water column (case of the explosion S8), rather than on the seabed (case of the explosion S7), even if the charge detonated in water is of smaller weight.

C. Spectral Analysis of the Signals

Spectral analysis was carried out through the estimation of the power spectral density (PSD) for the signals recorded by the

shock gauge transducer T11 and the hydrophone H240. Note that the signals recorded by the hydrophone H240 were not clipped. The PSDs were first calculated by considering a time window of 10 s and a resolution of 0.2 Hz (with 50% overlapping). Fig. 12 provides an illustration of the results obtained for the signals generated by the detonation of different TNT-equivalent charge weights (namely, 80 and 200 kg) on the seabed at the two different experiment sites (labeled 3TY and 3TZ; see Fig. 1).

We note the frequency peak associated with the first bubble period for each explosion, although the resolution of 0.2 Hz is not really optimal for processing the highly noisy signals provided by the shock transducer T11. This frequency peak is ~ 2.5 Hz for the explosions S1 and S2, ~ 3.3 Hz for the explosion S3, and ~ 1.9 Hz for the explosion S7.

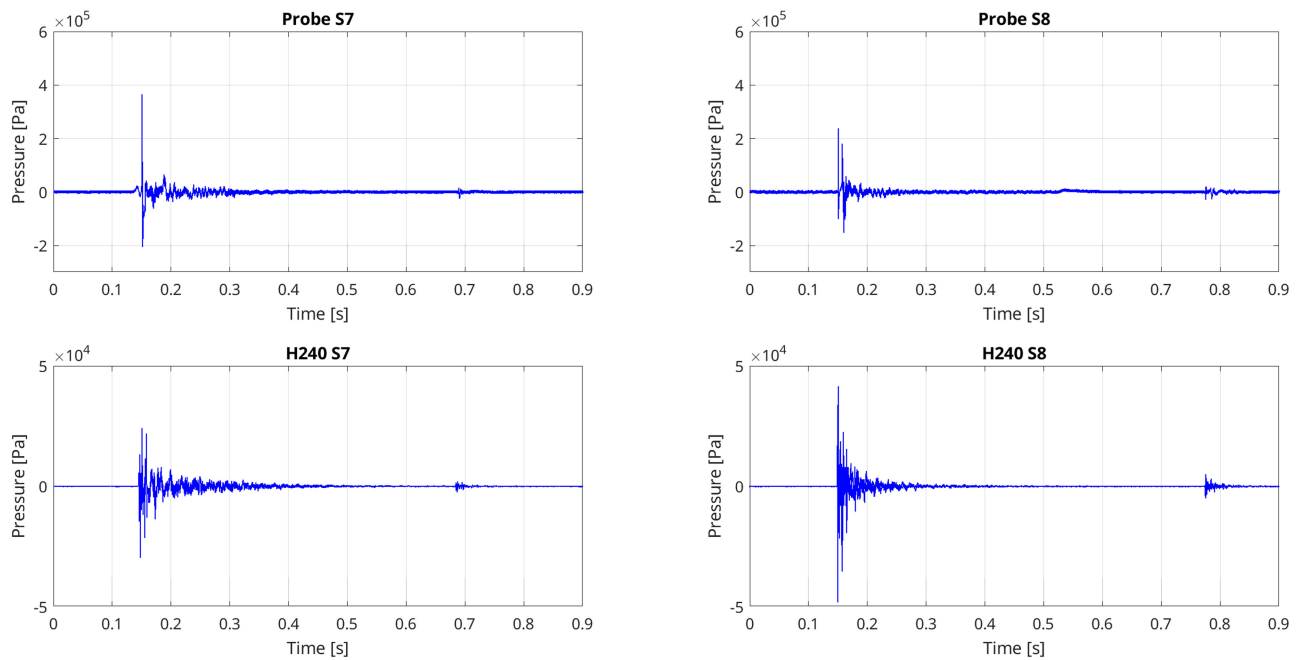


Fig. 11. Signals recorded by the shock transducer T11 (top) and by the hydrophone H240 (bottom), and generated by (left) the explosion of a 200-kg TNT-equivalent charge on the seabed (S7), and by (right) the explosion of an 80-kg TNT-equivalent charge located in a container in the water column (S8), at the experiment site 3TY. For both explosions, the transducer T11 was located at ~ 250 m and the hydrophone H240 at ~ 2840 m from the source.

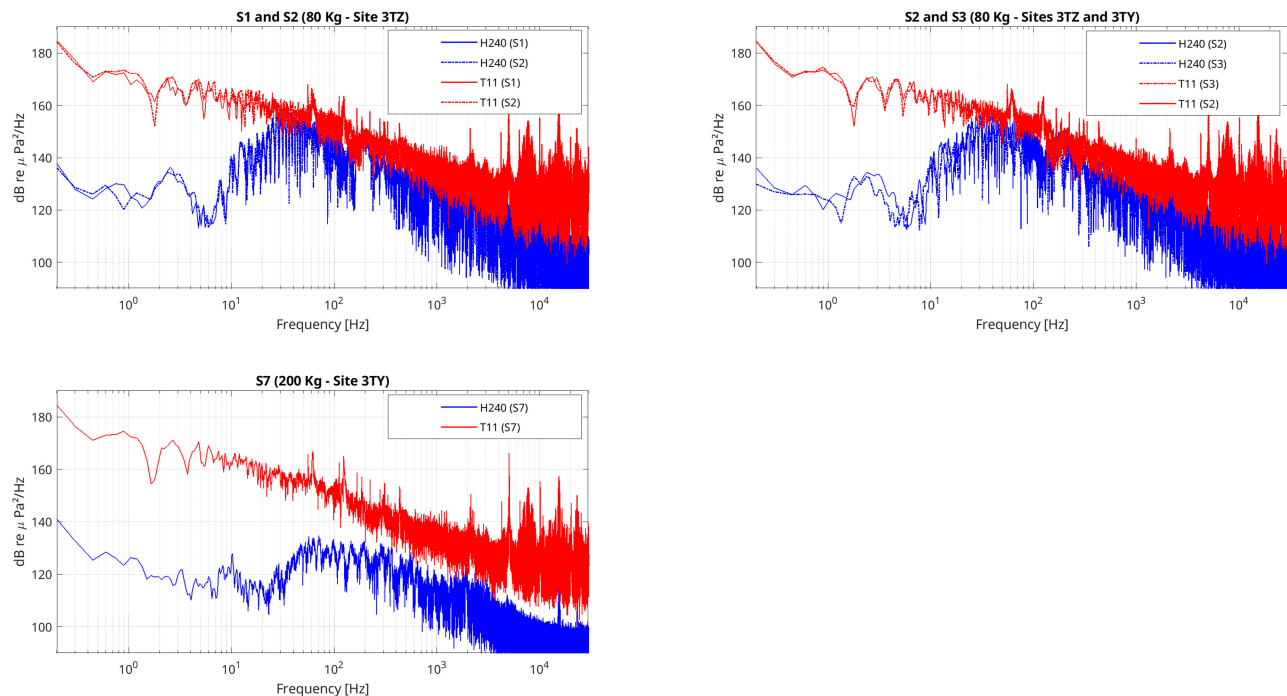


Fig. 12. Spectra (PSD) of the signals recorded by the shock gauge transducer (red curves) and the hydrophone H240 (blue curves) and generated by (a) the explosions S1 and S2 corresponding to 80-kg TNT-equivalent charges located at the 3TZ site, (b) the explosions S2 and S3, corresponding to 80-kg TNT-equivalent charges located at the 3TZ site and the 3TY site, respectively, and (c) the explosion S7 corresponding to a 200-kg TNT-equivalent charge located at the 3TY site. The shock transducer is located at ~ 160 m from the source S1, ~ 122 m from S2, ~ 110 m from S3, and ~ 239 m from S7, respectively. The hydrophone is located at ~ 408 m from the source S1, ~ 391 m from S2, ~ 326 m from S3, and ~ 2837 m from S7, respectively.

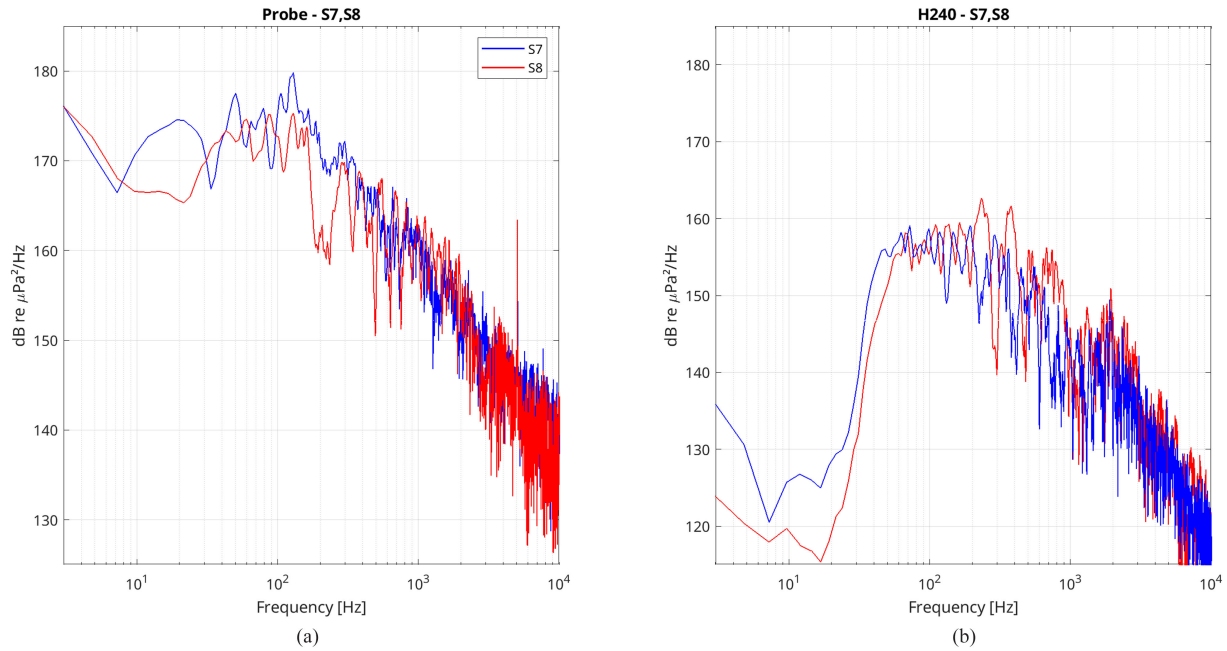


Fig. 13. PSD of the signals (shown in Fig. 11) recorded by (a) the shock gauge transducer T11 and (b) the hydrophone H240, located at ~ 250 and ~ 2840 m, respectively, from the sources. The explosions S7 and S8 of the charges of 80-kg TNT-equivalent weight were located on the seabed and in the water column, respectively.

The spectra (represented here in log scale) exhibit different other interesting features. First, the signal spectra are consistent for a given charge detonated at the same place [see Fig. 12(a)].

Second, whatever the charge weight and wherever the explosion location, the spectra of the signals recorded by the shock transducer (located “close” to the explosion) are quite similar and relatively constant between 0 and 300 Hz. For frequencies above 300 Hz, the spectra exhibit a significant drop.

Finally, whatever the charge weight and wherever the explosion location, the hydrophone, although having a good sensitivity at LF, could hardly record the components with frequencies below 30 Hz. Indeed, the LF wave propagation hardly occurs in the water column due to the waveguide cutoff frequencies.

It is interesting to exhibit the differences in the spectra of the signals generated by an explosion on the seabed and by an explosion in the water column. Contrary to the previous results shown in Fig. 12, the PSDs were then calculated by considering a shorter time window of 1 s and a resolution of 2 Hz (with 50% overlapping), to remove as much as possible the impact of the noise of the shock transducer on the spectra. Fig. 13 shows that a detonation on the seabed generates lower frequencies (globally, up to 30 Hz) than a charge detonation in the water column.

It is interesting to further investigate the explosion-induced signals, and more specifically to estimate the spectral contribution of the shock wave and the bubble pulse, respectively, to the global spectra. The goal is to discriminate the signal that may most contribute to the LF that are of interest for seismic risk assessment.

Noting that the shock wave signal and the bubble pulse signal only last a few microseconds, and that they are well separated in time, we could remove the bubble pulse signal from the whole measured signal to keep only the shock wave signal.

Subsequently, the PSDs were estimated independently for the shock wave signal alone and for the whole signal by considering a time window of 10 s and a resolution of 0.2 Hz (with 50% overlapping).

Fig. 14 shows that the shock wave signal mostly contributes to the high-frequency components of the whole spectrum (frequencies above 100 Hz), whereas the first bubble pulse signal contributes to the LF part (below 100 Hz with a peak around 30 Hz), which is consistent with information reported in the literature (e.g., [23]). Because of its contribution to the lower frequency part, the bubble pulse signal may be the most appropriate candidate to possibly generate seismic risks, in particular in the presence of sedimentary basins. Indeed, the sedimentary basins may lower the frequency content of the signals while locally amplifying their amplitude. This is the well-known site effect observed in seismology that can damage the buildings.

V. SEISMIC EXPLOSION-INDUCED SIGNALS RECORDED ON LAND

Before assessing seismic risks induced by large underwater explosions, it is important to gain insight into the seismic signals recorded on land, and to investigate the impact of the environment properties and the effect of the charge characteristics. This is the purpose of this section.

To study the impact of the environment and the effect of the propagation paths, we first analyze, for a given explosion, the seismic signals recorded by the network of the 20 seismic stations deployed all along the coast of the Rade d’Hyères. Additionally, to study the effect of the charge weight, we analyze, for a given station, the seismic signals induced by the eight explosions. The impact of the location of the source, namely on

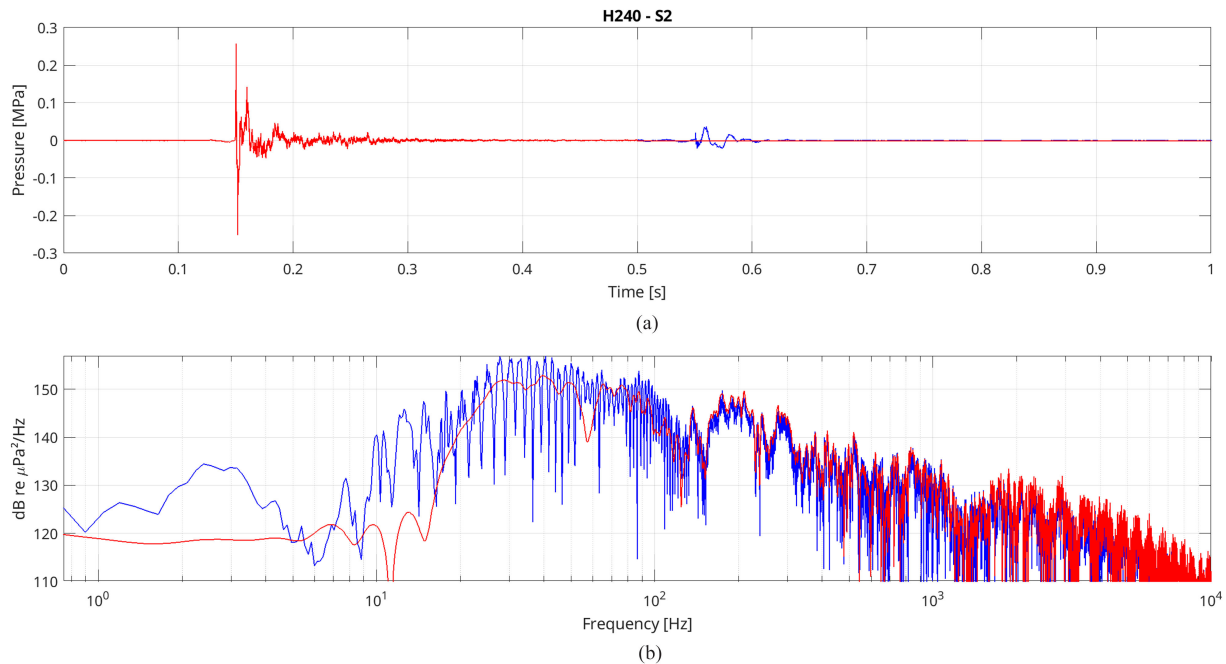


Fig. 14. (a) Pressure-time signatures of the shock wave alone (red) and of the shock wave together with the first bubble pulse (blue) measured by the hydrophone H240; and (b) associated spectra. The hydrophone was located at ~ 391 m from the explosion S2 corresponding to a charge weight of 80-kg TNT-equivalent.

the seabed or in the water column, is also investigated. Besides being relevant for establishing a prediction law for the seismic risks, some of these results will also provide valuable data for validating the numerical modeling developed in [3].

A. Influence of the Geological Environment on the Seismic Signals

The seismic ground motion, generated by the explosions S1–S8 (see Table I), was recorded by the network of 20 three-component velocimeters and accelerometers deployed all along the coast of the Rade d’Hyères (see Fig. 1, and Table II in Appendix 1). To study the impact of the environment on the seismic signals arriving at the land coast, we compare, for a given explosion, the signals recorded by the 20 stations.

For the sake of illustration, the vertical (Z) and horizontal (E, N) components of the seismic signals induced by the explosion S6 and recorded by the network are displayed in Fig. 15. Note that the traces are ordered azimuthally as listed in Table II, and that the color for each seismogram refers to the color scale used in Fig. 2.

We observe that the global signal waveforms and durations greatly differ according to the explosion-station distance, and according to the ground properties along the propagation path as well. The sediment thickness seems to have a significant influence. Indeed, for the stations installed on sites with several meters of sediments below (i.e., the stations PS09–PS16, corresponding to the traces in cyan, blue, pink, and red colors in Fig. 15), the first P-wave arrival is not as impulsive as the one observed at the other sites.

Most importantly, the signal duration is much longer, with the presence of late dispersive signals with a very LF content and, for

some stations, large amplitude. Although these characteristics are specific to the well-known site effects (e.g., [44] and [45]) induced by the sedimentary basin, no strong conclusion can be drawn from the observed differences in the signal amplitudes. Indeed, several factors, including the source-station distance and the conditions of the station setup on the rocky or sedimentary sites, may also impact the wave amplitudes.

B. Influence of the Characteristics of the Explosive Charges on the Seismic Signals

To study the impact of the weight and the location of the explosive charges on the seismic signals arriving at the land coast, we compare, for a given station, the signals induced by the eight explosions.

Fig. 16 shows the vertical component of the ground acceleration induced by each explosion (S1–S8) and recorded at the station PS05 (Fig. 1).

For a given location for explosions (either 3TY, or 3TZ) and for similar conditions (i.e., located on the seafloor), the signals are consistent.

The larger the charge weight, the larger the ground acceleration induced by all the waves, namely the direct wave arriving at ~ 0.5 s after each explosion, the wave associated with a reflection between the sea bottom and the sea surface and arriving at ~ 0.6 – 0.7 s, and the diffracted seismic waves (coda). For the source-station PS05 configuration, the relationship between the charge weight W (in kilograms TNT-equivalent) and the ground acceleration A (in nm/s^2) induced by the reflected wave can be derived from the signals (see Fig. 16)

$$A = 5.52 \cdot 10^5 + 0.08 W. \quad (4)$$

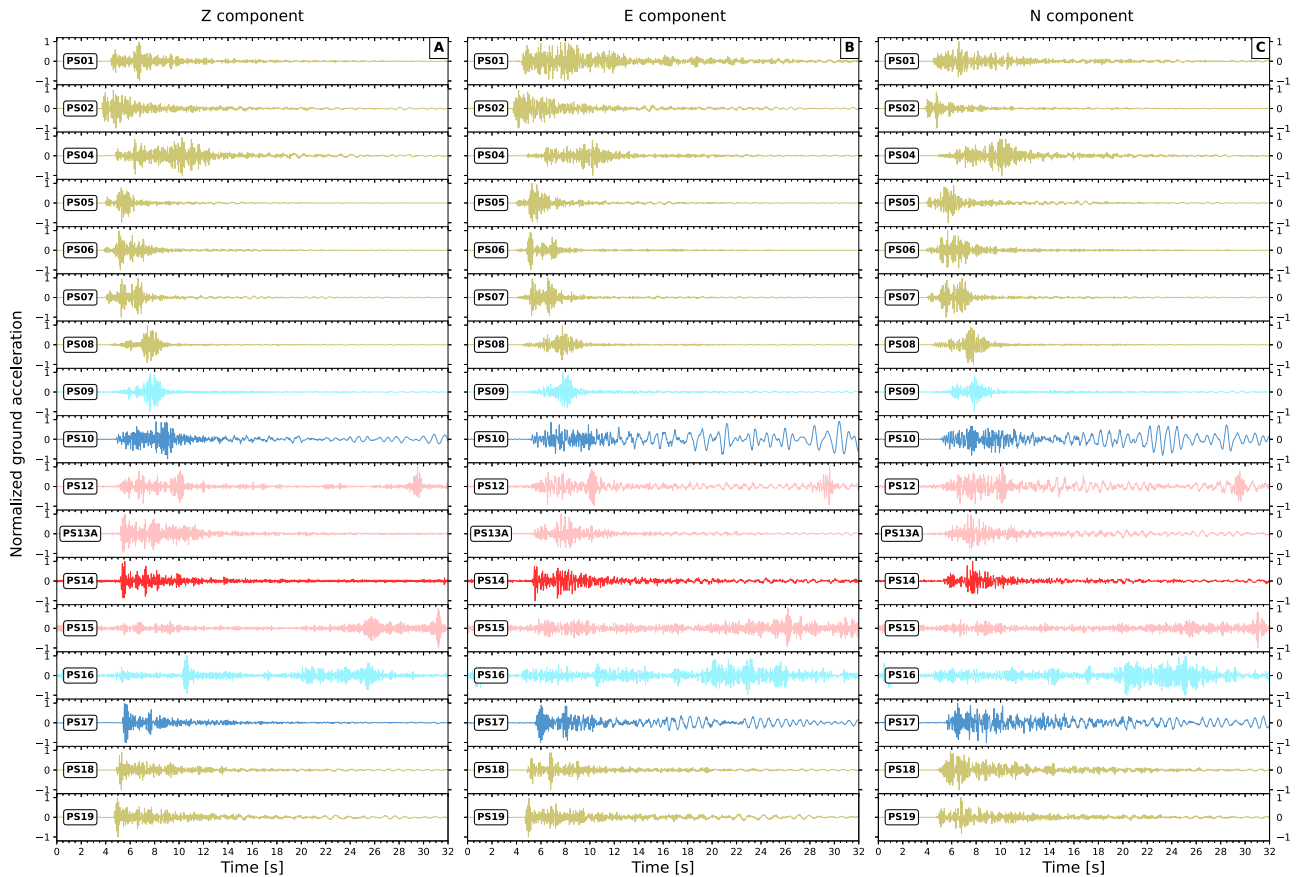


Fig. 15. Three-component ground accelerations induced by the explosion S6 (corresponding to a 400-kg TNT-equivalent charge located at the site 3TY), and recorded at the stations PS01–PS19 (see Fig. 1). The amplitude of the signals is normalized by the maximum amplitude of the corresponding ground acceleration. The signals are lowpass filtered at 20 Hz. The colors refer to the scale used in Fig. 2, i.e., for instance, the sandy color gathers all sites characterized by a sediment thickness of 0–1 m (namely, PS01–PS08, PS18, PS19), whereas the red-pink and blue colors refer to sites with a thick sedimentary layer. All traces are plotted with the same origin time (around the detonation time), and the amplitudes are graphically clipped between $\pm 5 \text{ mm}\cdot\text{s}^{-2}$ for clarity of display.

Finally, comparison between the signals generated by the explosions S3 and S8 (both corresponding to a 80-kg TNT-equivalent charge) highlights the fact that an explosion in the water column generates much less seismic energy than an explosion on the seabed. The fact that the charge is detonated directly on the seafloor, and not close to the seafloor as it is the case in [25], makes the coupling between the source and the seafloor very efficient. This conclusion is supported by the presence of blast marks observed on the images provided by multibeam echosounders and sidescan sonars [46].

C. Spectral Analysis of the Signals

Spectral analysis was carried out through the estimation of the PSD of the vertical component of the ground accelerations recorded at the station PS05 (see Fig. 16).

Fig. 17 clearly highlights that the detonations of charges of weight larger than 80-kg TNT-equivalent generate globally similar spectral responses for the vertical ground-acceleration components recorded on the shoreline. However, the amplitudes of the spectral responses increase with increasing charge weight. The same trend is observed for the horizontal component at various stations as well.

Whatever the source, the PSDs exhibit the most energetic peak in the 5–10-Hz frequency range that is likely associated with bulk wave propagation. A secondary peak is observed in the 0.8–2-Hz frequency range, but only for the largest charges. This peak is likely associated with surface wave propagation. The two peaks have almost the same shape, namely a sharp increase in amplitude (on the LF part) followed by a slow decay in amplitude (on the HF part).

From Fig. 17, it is also interesting to note that for a given charge weight (here, 80-kg TNT-equivalent), a charge detonation in the water column (namely, S8) generates globally less energetic seismic signals than a charge detonation on the sea bottom (namely, S3), in particular in the 2–30-Hz range that is of primary importance for the land infrastructures. This trend, confirmed by observations at the different stations along the coast (see Fig. 18), is consistent with the fact that the coupling between the source and the seafloor is more efficient when the explosive charge lies on the seabed.

This suggests that the countermining in the water column would minimize the explosion-induced effects on the buildings located on the coasts. However, the ground properties seem to largely affect the local amplitudes of the higher frequency components of the signals (see, for instance, for the frequencies

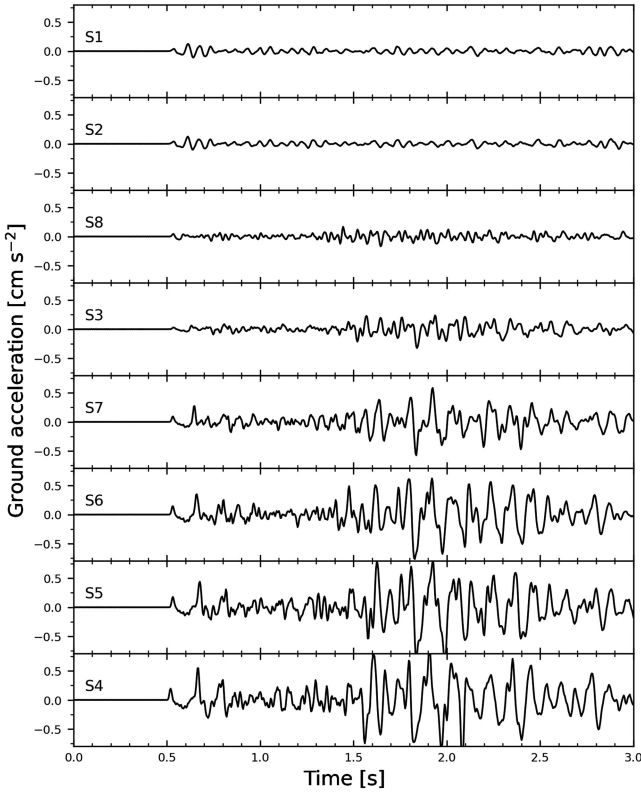


Fig. 16. Vertical component of the ground acceleration, generated by the sources S1–S8, and recorded by the velocimeters at the station PS05. The traces are ordered from the top to the bottom as follows: the signals generated by the two explosions S1 and S2 (corresponding to an 80-kg TNT-equivalent charge) located at the site 3TZ, then the signal generated by the explosion S8 (corresponding to an 80-kg TNT-equivalent charge) located at the site 3TY in the water column, and finally the signals generated by the explosions located at the site 3TY on the seafloor, from the lowest charge (i.e., S3, corresponding to an 80-kg TNT-equivalent charge) to the largest one (i.e., S4, corresponding to a 680-kg TNT-equivalent charge). The amplitudes are graphically clipped between $\pm 8 \text{ mm}\cdot\text{s}^{-2}$ for clarity of display.

above 80 Hz in Fig. 18). Indeed, while a soft soil attenuates the energy carried by the seismic signal close to the shore (see, for instance, the signals at the station PS19), a rocky ground seems to better preserve the HF energy propagation (see, for instance, the signals at the stations PS02, PS05A, and PS09).

VI. ASSESSMENT OF THE SEISMIC RISKS INDUCED BY THE UNDERWATER EXPLOSIONS THROUGH CHARGE WEIGHT/SEISMIC MAGNITUDE RELATIONSHIPS

As mentioned in the Introduction, the main goal of this study is to assess the seismic risks induced by the detonation of large-charge historical ordnance in a shallow water environment. We propose to rely on the analogy between small earthquakes and large explosions, and to make use of the seismic magnitude [2] as the metric for assessing these risks. Here, the goal is to derive relationships between the charge weight and the magnitude of the seismic event induced by the underwater explosion located on the seabed or in the water column.

Moreover, in the perspective of developing a decision support tool, it is relevant to check whether we can rely on the seismic

magnitudes derived only from permanent seismic networks located in the far field of the explosions to assess what happens in the near-field of large underwater explosions. Comparison of the magnitude derived from the signals induced by each explosion and recorded by our temporary stations with the magnitude derived from the signals recorded by permanent stations can provide useful insights.

To properly derive the empirical laws that relate the charge weights to the seismic magnitudes induced by the explosions, information on the source (namely, the charge weight, the date/time, and the location of the explosion), as well as information on the corresponding induced seismic signals, have to be as reliable as possible. In addition, to constrain these empirical laws as well as possible, a significant amount of data is required.

Accordingly, in support of the eight explosions already considered in this work, we selected 35 other underwater explosions. Eight explosions were performed in 2016 in the Grande Rade de Toulon (close to the Rade d'Hyères) within the POSA project; they are not reported in this article, but for these explosions the location and the weight of the charges are accurately known. Among the explosions reported in 2015–2016 in the French Navy's registers, 27 could be associated with known charges and could be clearly identified within the seismological database of the French permanent network RESIF [48]. Analysis of these seismological recordings allowed us to obtain the location of the explosions and the associated magnitudes (see Tables III and IV in Appendix 2).

For the sake of brevity, we do not describe here in detail the way of obtaining the magnitude of a seismic event. Indeed, the standard procedure routinely used to analyze regional seismic events is coded in SeisComp3 [49] following the definition of a local magnitude M_{LV} [2] that is an updated version of Richter's proposition [50].

The magnitude M_{LV} is usually deduced from the maximum amplitude A of the vertical component of the ground displacement recorded at a station located at a regional distance Δ (between 30 and 500 km) from the source

$$M_{LV} = \log(A) - \log(A_0) + c \log(\Delta). \quad (5)$$

The parameters $\log(A_0)$ and c have been adapted for the south-eastern part of France from a large dataset of events with magnitude 1–4 recorded at the RESIF permanent stations. To limit the influence of both the source process and the medium heterogeneities within the region under consideration, the magnitude of a seismic event is traditionally calculated as an average of the magnitudes obtained for all the available recordings [2]. As most of the stations of the RESIF network are stations located on rock outcrops, the magnitude is free of site-effect influences.

Accordingly, for the case of a charge detonation on the seabed, the empirical law for the relationship between the charge weight W (in kg TNT-equivalent) and the seismic magnitude M_{LV} was found to be

$$M_{LV} = 0.28 \log_{10}(W) + 1.83 \quad (6)$$

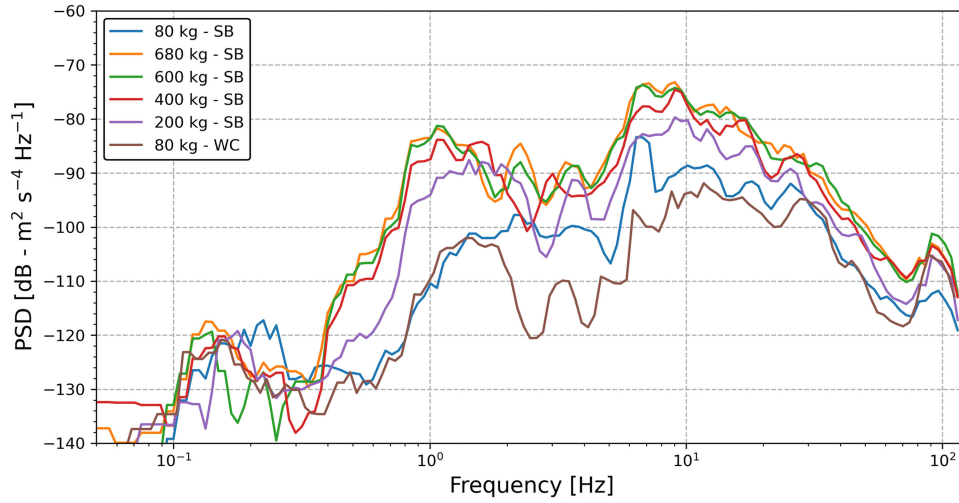


Fig. 17. PSDs of the vertical ground-acceleration components induced by the explosions S3–S8 (located at the site 3TY) and recorded by a velocimeter at the station PS05. The PSD associated with the detonation in the water column (WC) is represented by the brown curve, whereas the PSDs associated with the detonations on the seabed (SB) are represented by different colored curves.

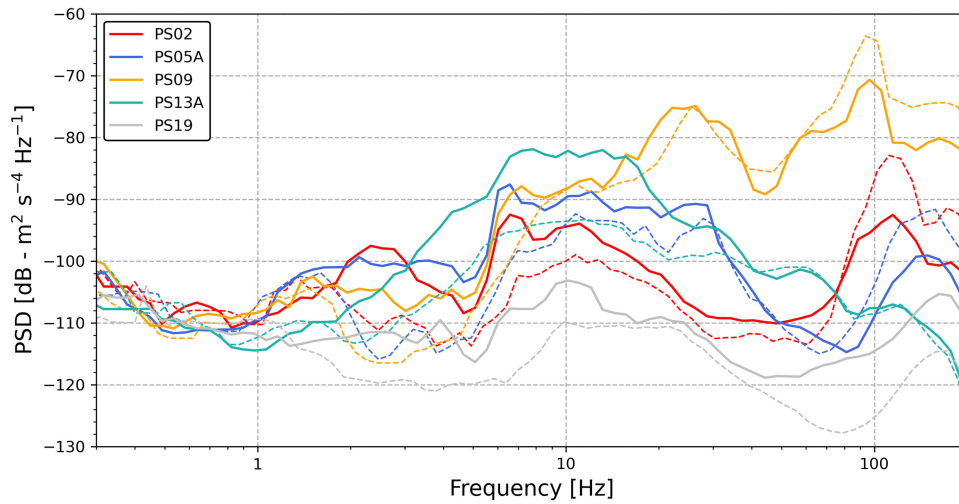


Fig. 18. PSDs of the vertical ground-acceleration components induced by the explosions S3 and S8 (located at the site 3TY, and both corresponding to a charge weight of 80-kg TNT-equivalent), and recorded by the DSU3-SA accelerometers at the different stations along the coast. The PSDs associated with the charge detonation in the water column (S8) are represented by the dashed curves, whereas the PSDs associated with the charge detonation on the seabed (S3) are represented by the solid curves.

with a standard deviation of 0.045, whereas for the case of a charge detonation in the water column

$$M_{Lv} = 0.30 \log_{10}(W) + 1.33 \quad (7)$$

with a standard deviation of 0.035.

These two empirical laws follow the same trend, but with a shift of 0.5 in magnitude (see Fig. 19). This result confirms that much less energy is transmitted downwards into the ground when the explosion occurs at a shallow water depth since part of the source energy is transferred to the air-shock wave [51]–[53].

From Fig. 19 and Appendix 2 (see Tables III–V), we notice that the countermining of explosive devices of large charge

weights (from 80- up to 680-kg TNT-equivalent) has induced seismic events with an equivalent magnitude of 2.9 at most, which is rather low to prevent any large damage to nearby masonry structures (see Appendix 3).

From Fig. 19, we also notice that the seismic magnitudes induced by the smallest charges (namely of 80-kg TNT-equivalent) are pretty well predicted by the empirical laws, whereas those induced by the largest charges detonated on the seabed are slightly underestimated. Further work is definitely needed to better understand the interaction of the explosions with the seabed and with the induced seismo-acoustic wave propagation, to define an optimized methodology to better assess seismic

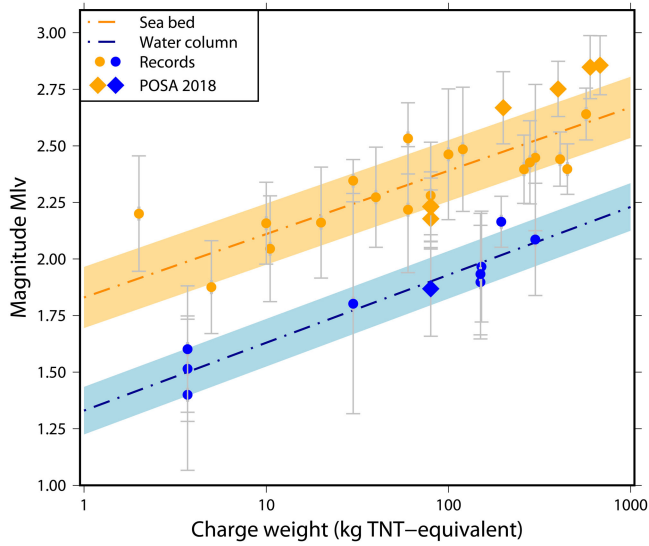


Fig. 19. Estimation of the magnitude of the seismic events (with associated uncertainties) as a function of the charge weight, when the charges are located (orange line) on the seabed, or (blue line) in the water column. The standard deviation associated to each linear regression is also shown.

risks induced by large underwater explosions in shallow water environments.

VII. CONCLUSION

The main goal of the work, presented here in a two-companion paper, is to pave the way for assessing in a reliable manner the risk of building damage on the adjacent shore, induced by the detonation of large-charge historical ordnance (of between 80- and 680-kg TNT-equivalent weight) in variable shallow water environments with a water depth less than 50 m. We suggest to quantify the risk assessment through the local seismic magnitude induced by the explosions. Beforehand, the relationship between the large charge weight and the seismic magnitude has to be investigated and derived for the case of a detonation on the seabed and for the case of a detonation in the water column.

In this article, we have investigated experimentally this relationship using a coupled seismo-acoustic approach within the framework of a UXO clearance (countermining) campaign conducted in December 2018 in the Rade d'Hyères (France), in the Mediterranean Sea. Hydro-acoustic and seismic recording systems have been deployed to record the explosion-induced waves in water and the seismic signals on the land coast, respectively. Analysis of the acoustic and seismic data, coupled to information provided by geological surveys, has thus enabled to draw preliminary conclusions regarding the risk assessment with respect to the inland infrastructures.

The detonation of a charge in the water column globally generates signals of higher amplitudes for both the shock wave and the bubble pulse than a detonation on the seabed. The shock wave mostly contributes to the high-frequency components of the whole spectrum (frequencies above 100 Hz), whereas the first bubble pulse generates energetic LF (below 100 Hz with a peak around 30 Hz). As a result, the first bubble pulse is the

main event that may be involved in land risks, in particular in the damages to buildings that are sensitive to these LF.

The detonation of a charge on the seabed generates seismic signals of much lower frequencies (up to 30 Hz) and of higher amplitudes than the detonation of a charge of similar weight in the water column. These LF components propagate better in the seabed than in the water column.

Moreover, the larger the charge weight, the higher the amplitude of the seismic signals. The ground acceleration is linearly related to the charge weight. However, besides the explosion-land distance, the ground properties seem to also affect the signals. On one hand, unconsolidated sediments can make the global signal duration much longer and may favor the presence of late dispersive signals with a very LF content and a possibly large amplitude (site effect). On the other hand, the ground properties may affect the local amplitudes of the higher frequency components of the signals. Indeed, while a soft soil attenuates the energy carried by the acoustic signal converted into a seismic signal close to the shore, a rocky ground seems to better preserve the high-frequency energy propagation (typically, above 30 Hz).

From these experiments, and with the help of additional recordings provided by a permanent station network, we have been able to derive two empirical laws that relate the charge weight and the explosion-induced seismic magnitude, for the case of a charge detonation in the water column and for the case of a charge detonation on the seafloor. These two empirical laws follow the same trend, but with a shift of 0.5 in magnitude. Indeed, much less energy is transmitted downwards into the ground when the explosion occurs at a shallow water depth. This suggests that, compared to a countermining on the seafloor, a countermining in the water column is preferable since it would minimize the explosion-induced effects on the buildings located on the coast. However, wherever their location, the charge detonations (up to 680-kg TNT-equivalent) have generated seismic events of at most magnitude 2.9 on the Richter scale. The magnitudes are low enough to prevent any large damage to the nearby inland infrastructures.

It is worth noting that all these conclusions are valid for the local shallow water environment considered in this study, but not necessarily valid for other coastal environments. More work is definitely needed to strengthen these preliminary conclusions.

Moreover, the work presented in this article has to be considered as a preliminary work on the seismic risks induced by the detonation of large charges in very shallow environments, since questions are still open. For instance, the issue of the influence of the seabed on the on-seabed explosion needs to be addressed in the future.

As already pointed out, accounting for the coupling between the acoustic and seismic wave propagation is essential when LF propagation is involved in shallow water configurations, because the presence of sedimentary basins may have a great influence on wave propagation, as is well known in seismology. A better understanding of the physics of the seismo-acoustic wave propagation in a variable shallow marine environment could also help in better interpreting the real data. This is the goal

TABLE II
DETAILED LIST OF THE SEISMIC INSTRUMENTS DEPLOYED DURING THE EXPERIMENTS ALL ALONG THE COAST OF THE RADE D'HYÈRES (SEE FIG. 1)

Instrum. label	Latitude (°)	Longitude (°)	Altitude (m)	Recording type
PS01	43.0003	6.204	2	Velocimeter Guralp CMG40-T
PS01H	43.0003	6.204	14	Velocimeter Guralp CMG40-T
PS02	43.0253	6.242	23	(Digital Sensor Unit Sercel) DSU3-SA accelerometer
PS04	43.0243	6.43917	9	DSU3-SA accelerometer
PS05	43.088	6.36333	48	Velocimeter Guralp CMG40-T + accelerometer Kinematics ES-T
PS05A	43.088	6.36333	48	DSU3-SA accelerometer
PS06	43.1007	6.324	2	DSU3-SA accelerometer
PS07	43.1097	6.30967	4	Velocimeter Guralp CMG-6T
PS08	43.1215	6.27133	1	Velocimeter Guralp CMG-6T
PS09	43.1175	6.2495	2	DSU3-SA accelerometer
PS10	43.1175	6.206	0	Velocimeter Guralp CMG-6T
PS12	43.093	6.1635	2	Velocimeter Guralp CMG40-T
PS13	43.0753	6.15267	2	Velocimeter Guralp CMG40-T
PS13A	43.0753	6.15267	2	DSU3-SA accelerometer
PS14	43.0652	6.15067	0	Velocimeter Guralp CMG40-T
PS15	43.0572	6.14767	2	Velocimeter Guralp CMG-6T
PS16	43.0475	6.14933	2	Velocimeter Guralp CMG40-T
PS17	43.0527	6.13333	1	DSU3-SA accelerometer
PS18	43.0342	6.16333	12	Velocimeter Guralp CMG-6T
PS19	43.0328	6.17283	7	DSU3-SA accelerometer

Note that the instrument labeled PS01H is located at the top of the bell tower of the Ste-Anne Church on the Porquerolles Island (see Fig. 7).

of Part II of the paper [3] that focuses on the cross-validation between numerical simulations of realistic wave propagation and the real seismic data.

The work presented in a two-companion article only focuses on risks of damage to buildings and infrastructures on the adjacent shore. It does not address the risks of harming or disturbing marine life (e.g., [15]). These risks will be also under consideration in our future works.

APPENDIX 1

CHARACTERISTICS OF THE SEISMIC INSTRUMENTS

See Table II.

APPENDIX 2

CHARACTERISTICS OF THE COUNTERMINING EXPERIMENTS USED TO ESTABLISH THE EMPIRICAL RELATIONSHIPS BETWEEN THE CHARGE WEIGHTS AND THE SEISMIC MAGNITUDES INDUCED BY THE CHARGE EXPLOSIONS

See Table III–V.

APPENDIX 3

ILLUSTRATION OF THE IMPACT OF THE UNDERWATER EXPLOSIONS ON A NEARBY MASONRY STRUCTURE

For the sake of illustration of the seismic response on nearby civil engineering structures, two velocimeters were located at the top (station PS01H, placed at 12 m above the ground level) and the bottom (station PS01), respectively, of the bell tower of the Ste-Anne Church located on the Porquerolles Island (see Fig. 20). The structure has been chosen because of its ease of accessibility and because of the absence of tall concrete buildings in the surroundings. The church is located inside the small village of Porquerolles, on a rocky site with no evidence of wave amplifications due to site effects.

Fig. 21 shows the horizontal component of the peak ground acceleration (PGA) induced by the eight explosions S1–S8, and recorded at the stations PS01 and PS01H.

The motion amplification due to the structure is clearly seen. The PGA values of $\sim 1.2 \text{ cm/s}^2$ are obtained at the top of the bell tower for the largest charges (namely, 680- and 600-kg TNT-equivalent corresponding to explosions S4 and S5, respectively).

It has to be noted that the associated peak ground velocity (PGV) values of $\sim 0.4 \text{ mm/s}$ are slightly higher than the perception limit of vibrations by humans (between 0.1 and 0.3 mm/s).

TABLE III
AVAILABLE INFORMATION ON THE COUNTERMININGS CARRIED OUT IN 2015/2016 IN THE TOULON/HYÈRES AREA, AND COLLECTED AT PRÉFECTURE MARITIME DE TOULON BY SHOM

Date / Time	Charge weight (kg)	Seismic Magnitude - M_{L_v}	Location of the charge	Latitude	Longitude
20-01-2016T08:02	450	2.39	On seabed	43.074233	5.97735
09-02-2016T09:08	2	2.20	On seabed	43.071333	5.954333
09-02-2016T10:13	60	2.53	On seabed	43.071333	5.954333
11-02-2016T09:25	30	2.34	On seabed	43.071333	5.954333
29-03-2016T07:09	300	2.44	On seabed	43.3137	4.610867
30-03-2016T07:20	260	2.39	On seabed	43.324983	4.5977
12-05-2016T13:40	280	2.42	On seabed	43.31945	4.618467
20-05-2016T15:39	10.5	2.04	On seabed	43.06535	5.89215
31-05-2016T09:05	150	1.89	In water	42.5893	3.12195
01-06-2016T13:21	152	1.96	In water	42.5893	3.12195
02-06-2016T09:58	300	2.08	In water	42.5893	3.12195
07-06-2016T08:55	3.7	1.40	In water	43.083667	5.972
07-06-2016T09:13	3.7	1.51	In water	43.083667	5.972
07-06-2016T09:30	3.7	1.60	In water	43.083667	5.972
21-09-2016T10:25	195	2.16	In water	43.073167	5.959333
21-09-2016T14:38	570	2.64	On seabed	42.988367	6.310083
18-10-2016T12:39	410	2.44	In water	43.38185	4.98735
16-11-2016T07:33	30	1.80	In water	43.207	6.699667
15-01-2015T11:06	292	2.60	Unknown	43.400416	6.7421666
16-01-2015T10:39	462	2.58	Unknown	43.400416	6.7421666
10-02-2015T10:29	564	2.37	Unknown	43.3745	6.7616666
10-02-2015T14:04	678	2.63	Unknown	43.375483	6.7524833
10-05-2017T06:40	150	1.933	In water	43.63	7.32

Note that the location of those explosions could be determined only by using the RESIF permanent seismological network.

TABLE IV
INFORMATION ON THE COUNTERMININGS CARRIED OUT IN 2016 IN THE GRANDE RADE DE TOULON WITHIN THE POSA PROJECT (NOT REPORTED IN THIS ARTICLE)

Date /Time	Charge weight (kg)	Equivalent Magnitude - M_{L_v}	Location of the charge	Latitude	Longitude
18-11-2016T11:05:09	100	2.46	On seabed	43.0845	5.98133
18-11-2016T12:17:49	120	2.48	On seabed	43.0845	5.98133
18-11-2016T14:28:41	60	2.21	On seabed	43.0845	5.98133
18-11-2016T15:31:49	80	2.28	On seabed	43.0845	5.98133
25-11-2016T09:42:00	40	2.27	On seabed	43.0845	5.98133
25-11-2016T10:34:00	20	2.16	On seabed	43.0845	5.98133
25-11-2016T11:13:00	10	2.15	On seabed	43.0845	5.98133
25-11-2016T12:44:00	5	1.87	On seabed	43.0845	5.98133

TABLE V
INFORMATION ON THE COUNTERMININGS CARRIED OUT IN 2018 IN THE RADE D'HYÈRES WITHIN THE POSA PROJECT (REPORTED IN THIS ARTICLE)

Date /Time	Source	Charge weight (kg)	Equivalent Magnitude - M_{L_v}	Location of the charge	Latitude	Longitude
11-12-2018T13:13:29	S1	80	2.23	On seabed	43.075	6.24944
11-12-2018T14:03:03	S2	80	2.23	On seabed	43.075	6.24944
11-12-2018T15:28:20	S3	80	2.17	On seabed	43.04583	6.30361
12-12-2018T07:20:29	S4	680	2.85	On seabed	43.04583	6.30361
12-12-2018T08:10:44	S5	600	2.84	On seabed	43.04583	6.30361
12-12-2018T09:03:20	S6	400	2.75	On seabed	43.04583	6.30361
12-12-2018T09:48:35	S7	200	2.58	On seabed	43.04583	6.30361
12-12-2018T12:37:51	S8	80	2.01	In water	43.04583	6.30361



(a)



(b)

Fig. 20. (a) Ste-Anne church located on the Porquerolles Island. (b) Two velocimeters placed at the bottom and at the top of the bell tower, respectively.

The peak ground displacement values of less than $10 \mu\text{m}$, estimated from the recordings, are well below the assumed damage threshold for masonry structures [54], [55].

ACKNOWLEDGMENT

The authors warmly thank the Editor Emeritus N. Ross Chapman and three anonymous reviewers for their insightful and constructive reviews and for their highly valuable suggestions that greatly improved the article. This work was granted access to the seismic resources of Résif-Epos. Résif-Epos is a Research Infrastructure managed by CNRS-Insu. Inscribed on the roadmap of the Ministry of Higher Education, Research and Innovation, the Résif-Epos IR is a consortium of 18 French research organizations and institutions. Résif-Epos

benefits from the support of the Ministry of Ecological Transition. The RESIF data, used in the work presented here, come from <http://dx.doi.org/10.15778/RESIF.FR>. The authors greatly acknowledge the Préfecture de la Méditerranée, the Groupe des Plongeurs Démineurs and the Force de Guerre des Mines for their management of the two countermining operations. Shom/GHOA, and in particular X. Mathias, P. Guyomard, E. Brenon, H. Gauduin, M. Gosselin, J.-P. Boivin, and F. Jourdin, are also greatly acknowledged for the hydrographic and geological surveys. Semantic-TS provided onsite logistic support, realized the GPS points of the recorders, and chartered the measurement vessel Mousquemer piloted by P. Bernardi. X. Martin (Géoazur), Ph. Langlaude (CEREMA), M. Pernoud (CEREMA), and M. Perrault (CEREMA) are greatly acknowledged for their help with the seismic surveys. This article is dedicated to their late colleague D. Komatitsch (1970–2019).

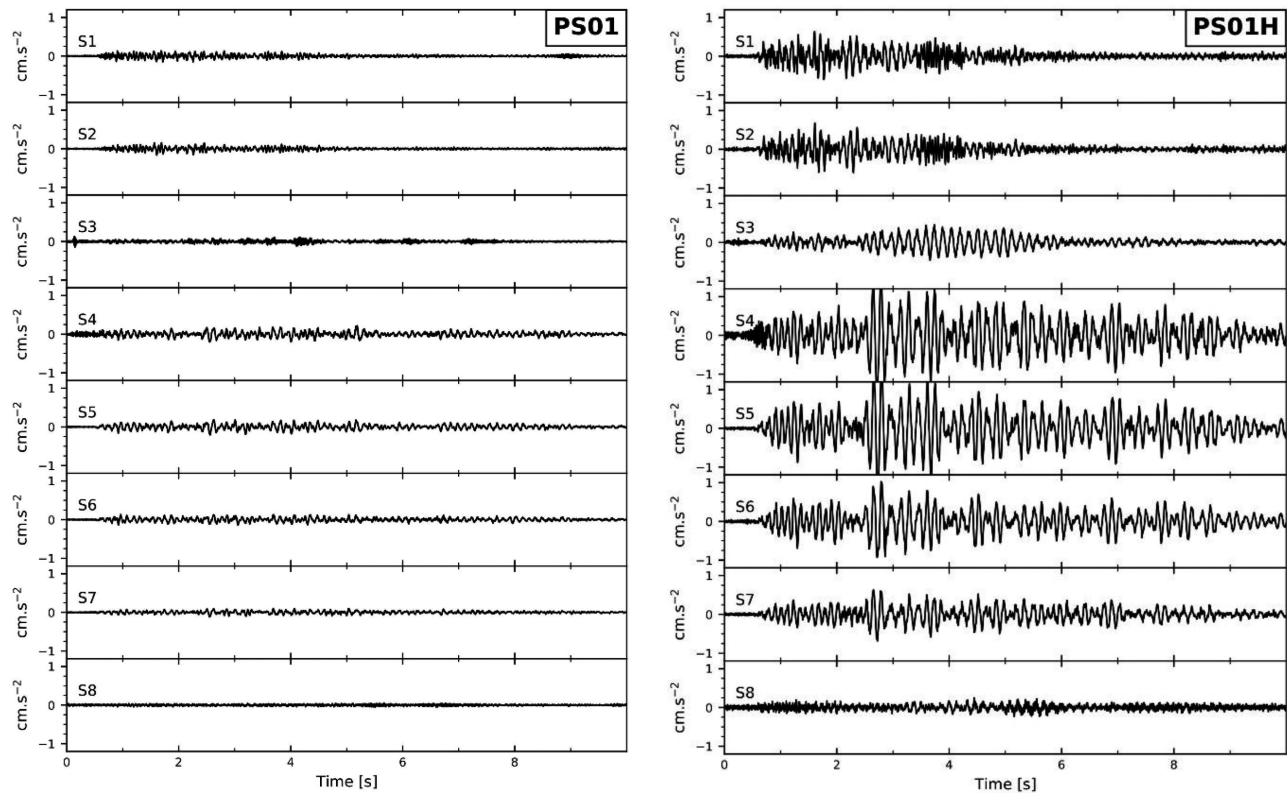


Fig. 21. Horizontal component of the PGAs, recorded at the bottom (PS01) and at the top (PS01H) of the bell tower of the Ste-Anne Church located on the Porquerolles Island, and induced by the eight explosions S1–S8.

REFERENCES

- [1] S.-H. Cheong, L. Wang, P. Lepper, and S. Robinson, "Characterisation of acoustic fields generated by UXO removal—Phase 2," Dept. Bus., Energy Ind. Strategy, Nat. Phys. Lab., Teddington, U.K., Rep. AC19, 2020.
- [2] P. Bormann, S. Wendt, and D. DiGiacomo, "Seismic sources and source parameters," in *New Manual of Seismological Observatory Practice 2*, P. Bormann Ed. Potsdam, Germany: Deutsches GeoForschungsZentrum, 2013, pp. 1–259.
- [3] N. Favretto-Cristini *et al.*, "Assessment of risks induced by countermining unexploded large-charge historical ordnance in a shallow water environment—Part II: Modeling of seismo-acoustic wave propagation," *IEEE J. Ocean. Eng.*, early access, 2021, doi: [10.1109/JOE.2021.3111791](https://doi.org/10.1109/JOE.2021.3111791).
- [4] D. Bowers and N. D. Selby, "Forensic seismology and the comprehensive-nuclear-test-ban treaty," *Annu. Rev. Earth Planet. Sci.*, vol. 37, pp. 209–236, 2009.
- [5] A. Douglas, *Forensic Seismology and Nuclear Test Bans*. Cambridge, U.K.: Cambridge Univ. Press, 2013.
- [6] K. D. Koper, T. C. Wallace, S. R. Taylor, and H. E. Hartse, "Forensic seismology and the sinking of the Kursk," *EOS Trans. Amer. Geophys. Union*, vol. 82, no. 4, pp. 37–52, 2001.
- [7] S. G. Kim and Y. Gitterman, "Underwater explosion (UWE): Analysis of the ROKS Cheonan incident," *Pure Appl. Geophys.*, vol. 170, pp. 547–560, 2013.
- [8] N. R. Chapman, "Measurement of the waveform parameters of shallow explosive charges," *J. Acoust. Soc. Amer.*, vol. 78, no. 2, pp. 672–681, 1985.
- [9] G. Nolet and L. M. Dorman, "Waveform analysis of Scholte modes in ocean sediment layers," *Geophys. J. Int.*, vol. 125, pp. 385–396, 1996.
- [10] A. G. Soloway and P. H. Dahl, "Peak sound pressure and sound exposure level from underwater explosions in shallow water," *J. Acoust. Soc. Amer.*, vol. 136, no. 3, pp. EL218–EL223, 2014.
- [11] J. B. Gaspin, J. A. Goertner, and I. M. Blatstein, "The determination of acoustic sources levels for shallow underwater explosions," *J. Acoust. Soc. Amer.*, vol. 66, no. 5, pp. 1453–1462, 1979.
- [12] Y. Gitterman, "Near-source audiovisual, hydroacoustic, and seismic observations of Dead Sea underwater explosions," *Combustion Explosion Shock Waves*, vol. 45, no. 2, pp. 218–229, 2009.
- [13] R. E. White and R. F. Mereu, "Deconvolution of refraction seismograms from large underwater explosions," *Geophysics*, vol. 37, no. 3, pp. 431–444, 1972.
- [14] K. S. Hunter and T. L. Geers, "Pressure and velocity fields produced by an underwater explosion," *J. Acoust. Soc. Amer.*, vol. 115, no. 4, pp. 1483–1496, 2004.
- [15] A. M. von Benda-Beckmann *et al.*, "Assessing the impact of underwater clearance of unexploded ordnance on harbour porpoises (*Phocoena phocoena*) in the Southern North Sea," *Aquatic Mammals*, vol. 41, no. 4, pp. 503–523, 2015.
- [16] H. Jones and A. R. Miller, "The detonation of solid explosives: The equilibrium conditions in the detonation wavefront and the adiabatic expansion of the products of detonation," *Proc. Roy. Soc. Lond. A*, vol. 194, pp. 480–507, 1948.
- [17] R. H. Cole, *Underwater Explosion*. Princeton, NJ, USA: Princeton Univ. Press, 1948.
- [18] D. E. Weston, "Underwater explosion as acoustic sources," *Proc. Phys. Soc.*, vol. 76, pp. 233–249, 1960.
- [19] F. A. Costanzo, "Underwater explosion phenomena and shock physics," in *Proc.* pp. 917–938, 2010.
- [20] A. B. Arons, "Underwater explosion shock waves parameters at large distances from the charge," *J. Acoust. Soc. Amer.*, vol. 26, no. 3, pp. 343–346, 1954.
- [21] M. Laverne, "Emission by underwater explosions," *Geophysics*, vol. 35, no. 3, pp. 419–435, 1970.
- [22] N. R. Chapman, "Source levels of shallow explosive charges," *J. Acoust. Soc. Amer.*, vol. 84, no. 2, pp. 697–702, 1988.
- [23] Y. Gitterman, Z. Ben-Avraham, and A. Ginzburg, "Spectral analysis of underwater explosions in the Dead Sea," *Geophys. J. Int.*, vol. 134, pp. 460–472, 1998.
- [24] P. S. Wilson, D. P. Knobles, P. H. Dahl, A. R. McNeese, and M. C. Zeh, "Short-range signatures of explosive sounds in shallow water used for seabed characterization," *IEEE J. Ocean. Eng.*, vol. 45, no. 1, pp. 14–25, Jan. 2020.

- [25] J. R. Krieger and G. L. Chahine, "Acoustic signals of underwater explosions near surfaces," *J. Acoust. Soc. Amer.*, vol. 118, no. 5, pp. 2961–2974, 2005.
- [26] E. M. Salomons, B. Binnerts, K. Betke, and A. M. von Benda-Beckmann, "Noise of underwater explosions in the North Sea. A comparison of experimental data and model predictions," *J. Acoust. Soc. Amer.*, vol. 149, no. 3, pp. 1878–1888, 2021.
- [27] D. Rauch, "On the role of bottom interface waves in ocean seismo-acoustics: A review," in *Ocean Seismo-Acoustics: Low-Frequency Underwater Acoustics*, T. Aka and J. M. Berkson, Eds. New York, NY, USA: Plenum, 1986, pp. 623–641.
- [28] A. G. Soloway, P. H. Dahl, and R. I. Odom, "Modeling explosion generated Scholte waves in sandy sediments with power law dependent shear wave speed," *J. Acoust. Soc. Amer.*, vol. 138, no. 4, pp. EL370–EL374, 2015.
- [29] L. Wan, M. Badiey, D. P. Knobles, and P. S. Wilson, "The Airy phase of explosive sounds in shallow water," *J. Acoust. Soc. Amer.*, vol. 143, no. 3, pp. EL199–EL205, 2018.
- [30] T. V. McEvilly and S. J. William Stauder, "Effect of sedimentary thickness on short-period Rayleigh-wave dispersion," *Geophysics*, vol. 30, no. 2, pp. 198–203, 1965.
- [31] J. L. King and B. E. Tucker, "Observed variations of earthquake motion across a sediment-filled valley," *Bull. Seismol. Soc. Amer.*, vol. 74, no. 1, pp. 137–151, 1984.
- [32] P. Y. Bard and M. Bouchon, "The two-dimensional resonance of sediment-filled valleys," *Bull. Seismol. Soc. Amer.*, vol. 75, no. 2, pp. 519–541, 1985.
- [33] K. C. Meza-Fajardo, C. Varone, L. Lenti, S. Martino, and J.-F. Semblat, "Surface wave quantification in a highly heterogeneous alluvial basin: Case study of the Fosso Di Vallerano valley, Rome, Italy," *Soil Dyn. Earthq. Eng.*, vol. 120, pp. 292–300, 2019.
- [34] O. Morio, T. Garlan, X. Mathias, P. Guyomard, Y. Le Faou, and H. Gauduin, "ANR POSA : Rapport descriptif du modèle 3D géologique multi-paramètres de la Rade d'Hyères et de ses abords," (in French), SHOM, Brest, France, Final Rep., 2017.
- [35] J. Blanc, "Etude sédimentologie de la presqu'île de Giens et de ses abords," (in French), *Recueil des Travaux de la Station Marine d'Endoume*, vol. 33, no. 20, pp. 35–52, 1960.
- [36] A. Stéphanian and I. Thinin, "Evaluation des risques naturels littoraux—SCoT Provence Méditerranée—Evaluation des stocks sédimentaires littoraux—Prospection géophysique," (in French), Bureau de Recherches Géologiques et Minières, Orléans, France, Final Rep. BRGM/RP-64158-FR, 2014.
- [37] E. J. Conrath, T. Krauthammer, K. A. Marchand, and P. F. Mlakar, *Structural Design for Physical Security: State of the Practice*. Reston, VA, USA: SEI Amer. Soc. Civil, 1999.
- [38] A. S. Kumar, V. B. Rao, R. K. Sinha, and A. S. Rao "Evaluation of plastic bonded explosive (PBX) formulations based on RDX, aluminum, and HTPB for underwater applications," *Propellants Explosives Pyrotechnics*, vol. 35, no. 4, pp. 359–364, 2010.
- [39] W. D. Reid, "The response of surface ships to underwater explosions," Aeronaut. Maritime Res. Lab., DSTO, Melbourne, VIC, Australia, 1996, pp. 1–38.
- [40] J. Rajasekar, T. H. Kim, and H. D. Kim, "Visualization of shock wave propagation due to underwater explosion," *J. Vis.*, vol. 23, pp. 825–837, 2020.
- [41] H. F. Willis, "Underwater explosions—Time interval between successive explosions," in *Underwater Explosion Research*, vol. 2. Washington, DC, USA: ONR, 1941, pp. 13–33.
- [42] G. Barras, M. Souli, N. Aquelet, and N. Couty, "Numerical simulation of underwater explosions using an ALE method—The pulsating bubble phenomena," *Ocean Eng.*, vol. 41, pp. 53–66, 2012.
- [43] G. Bjarnholt, "Suggestions on standards for measurement and data evaluation in the underwater explosion test," *Propellants Explosives Pyrotechnics*, vol. 5, no. 2/3, pp. 67–74, 1980.
- [44] F. J. Sánchez-Sesma and F. Luzón, "Seismic response of three-dimensional alluvial valleys for incident P, S, and Rayleigh waves," *Bull. Seismol. Soc. Amer.*, vol. 85, no. 1, pp. 269–284, 1995.
- [45] V. M. Cruz-Atienza, J. Tago, J. D. Sanabria-Gómez, E. Chaljub, V. Etienne, J. Virieux, and L. Quintanar, "Long duration of ground motion in the paradigmatic valley of Mexico," *Sci. Rep.*, vol. 6, no. 1, 2016, Art. no. 38807, doi: [10.1038/srep38807](https://doi.org/10.1038/srep38807).
- [46] T. Garlan *et al.*, "Circular sedimentary figures of anthropic origin in a sediment stability context," *J. Coastal Res.*, vol. 85, pp. 411–415, 2018.
- [47] S. R. Kotha, D. Bindi, and F. Cotton, "Partially non-ergodic region specific GMPE for Europe and the Middle-East," *Bull. Earthq. Eng.*, vol. 14, pp. 1245–1263, 2016.
- [48] RESIF, "RESIF-RLBP French broad-band network, RESIF-RAP strong motion network and other seismic stations in metropolitan France. RESIF - Réseau Sismologique et géodésique Français," 1995, doi: [10.15778/RESIF.FR](https://doi.org/10.15778/RESIF.FR).
- [49] B. Weber *et al.*, "SeisComp3—Automatic and interactive real time data processing," *Geophys. Res. Abstr.*, vol. 9, 2007, Art. no. 09219.
- [50] C. F. Richter, "An instrumental earthquake magnitude scale," *Bull. Seismol. Soc. Amer.*, vol. 25, no. 1, pp. 1–32, 1935.
- [51] O. A. Godin, "Transmission of low-frequency sound through the water-to-air interface," *Acoust. Phys.*, vol. 53, pp. 305–312, 2007.
- [52] D. C. Calvo, M. Nicholas, and G. J. Orris, "Experimental verification of enhanced sound transmission from water to air at low frequencies," *J. Acoust. Soc. Amer.*, vol. 134, no. 5, pp. 3403–3408, 2013.
- [53] D. Wehner, U. P. Svensson, and M. Landrø, "Acoustic signals in air and water generated by very shallow marine seismic sources: An experimental study," *J. Acoust. Soc. Amer.*, vol. 147, no. 2, pp. 1092–1103, 2020.
- [54] D. D'Ayala, "Assessing the seismic vulnerability of masonry buildings," in *Handbook of Seismic Risk Analysis and Management of Civil Infrastructure Systems*, K. Goda and S. Tesfamariam, Eds., Sawston, U.K.: Woodhead Publishing, 2013.
- [55] S. Lagomarsino and S. Cattari, "Perpetuate guidelines for seismic performance-based assessment of cultural heritage masonry structures," *Bull. Earthq. Eng.*, vol. 13, pp. 13–47, 2015.

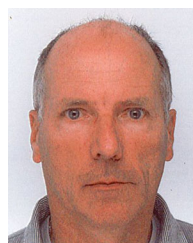


Nathalie Favretto-Cristini received the M.S. degree in mechanics and the Ph.D. degree in underwater acoustics from the Université de la Méditerranée, Marseille, France, in 1993 and 1997, respectively.

From 1997 to 1999, and then from 1999 to 2008, she was successively a Postdoctoral Fellow and a Researcher with the French National Centre for Scientific Research (CNRS), Laboratory of Modeling and Imaging in Geosciences, Pau, France. Since 2008, she has been a CNRS Researcher with the Laboratory of Mechanics and Acoustics, Marseille, France. From

2012 to 2017, she was the Deputy Director of this Laboratory. Her past and present research interests are focused on the interaction of waves with the interfaces in the sea bottom, and more specifically on seismo-acoustic wave propagation for underwater acoustics and seismic exploration applications.

Dr. Favretto-Cristini is a member of the American Society of Exploration Geophysicists, the European Association of Geoscientists and Engineers, and the French Society of Acoustics. She was a Co-Chief Scientist for the POSA project.



Thierry Garlan received the M.S. and Ph.D. degrees in geology from the University of Caen, Caen, France, in 1982 and 1985, respectively.

Since 1988, he has been an Expert Researcher in marine sedimentology and sediment dynamics modeling with the Service of Hydrography and Oceanography of the Navy (Shom), Brest, France. From 1988 to 1992, he was in charge of the development of nautical charts of atoll environments from satellite data. Since 2008, he has been the Head of the Department of Marine Geology, Shom. He has been the manager

of many research projects concerned with sediment dynamics and funded by the French Ministry of Research or the French Ministry of Defence. He has set up and coorganized many international conferences devoted to marine and river dunes dynamics and to coastal dynamics.

Dr. Garlan is a member of two French Expert Committees focused on Solid Earth (Commission Spécialisée Terre solide, CNRS/INSU and GT Terre solide ALLENI). He was the Lead Chief Scientist for the POSA project.



Olivier Morio received the M.S. degree in geography from the European Institute of Marine Sciences, Plouzané, France, in 2013, and the Ph.D. degree in marine geosciences from the University of South Brittany, Lorient, France, in 2017.

He then served as a Research Engineer with the Department of Marine Geology, Service of Hydrography and Oceanography of the Navy (Shom), Brest, France. He has been part of many research projects concerned with coastal dynamics and numerical modeling, especially in shallow water environments, that were funded by the French Ministry of Research or the French Ministry of Defence. Since 2018, he has been in charge of the onboard acoustic systems for Shom hydrographic fleet (multibeam echosounders, sub-bottom profilers, and acoustic Doppler current profilers). His current research interests include seabed acoustic backscattering and classification.



Xavier Demoulin received the M.S. degree in sciences of matter from École Normale Supérieure de Lyon, Lyon, France, in 1990, and the Ph.D. degree in marine geosciences from the University of Brest, Brest, France, in 2015.

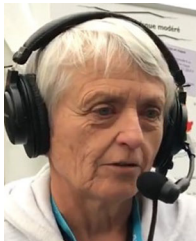
From 1995 to 2001, he was an Engineer with the Service of Hydrography and Oceanography of the Navy (Shom), Brest, France. In 2003, he created a small company named MAREE, located in Plémeur, France, which specializes in underwater acoustics and marine geophysics. Since 2003, he has been the Manager of MAREE.



Michel Arrigoni received the M.S. degree in mechanics and Ph.D. degree in energetics from the Université de Poitiers, Poitiers, France, in 2001 and 2004, respectively.

From 2005 to 2007, he was successively a Postdoctoral Fellow with the Institut National Polytechnique de Grenoble, Grenoble, France, and an Invited Researcher with the National Research Council Canada at the Industrial Material Institute of Boucherville, Montreal, QC, Canada. He got specialized on shock propagation in multilayered media. In 2007, he became an Assistant Professor with ENSTA Bretagne, Brest, France. Since 2016,

he has been a Full Professor. He develops research activities on shocks, impacts, and explosions with Institut de Recherche Dupuy de Lôme (IRDL, CNRS), Brest, France. He is currently the Team Leader of the "Fluid-Structure Interaction" Group, Brest, whose research activities concern effects characterization and mitigation of impacts and explosions.



Anne Deschamps received the Ph.D. degree in geophysics from Université de Paris VI, Paris, France, in 1986.

From 1979 to 1992, she was a Researcher in seismology with the Institut de Physique du Globe de Paris, Paris, France. From 1992 to 2002, she was in charge of the regional seismic network in Provence-Alpes-Côte d'Azur region (south-eastern part of France) at the Géoazur Laboratory, France. She developed accelerometric and broadband seismological observation. She is currently an Emeritus

Research Director with the French National Centre for Scientific Research (CNRS), France. Her research interests are mainly focused on the physics of earthquakes. They include the large earthquakes, seismicity, seismogenesis, and tectonics in the Mediterranean area, and also different geodynamical contexts like the large subduction of South America, the collision in Mongolia, and the rifting in Tanzania. She actively participated in the creation of the Corinth Rift Laboratory, namely the single transnational European Near Fault Observatory, that was recently integrated in EPOS (a Research European Infrastructure). Her current research interests concern the seismological site effects and the impact of seismic waves on buildings.

Dr. Deschamps was a Co-Chief Scientist for the POSA project.



Mickaël Bonnin received the M.S. degree in geology and geodynamics and Ph.D. degree in seismology from the University of Montpellier, Montpellier, France, in 2008 and 2011, respectively.

After a Postdoctoral Fellowship in seismology with the Géoazur Laboratory, University of Nice Sophia-Antipolis, Nice, France, he was hired as an Associated Physicist with the Laboratory of Planetology and Geodynamics, University of Nantes, Nantes, France, in 2014. Since then, he has been in charge of the NW array of the French broadband seismic network. His research interests mainly concern imagery and characterization of the deformation in the lithosphere and the uppermost mantle through study of seismic anisotropy and of low-intensity local seismicity.



Éric Beucler received the M.S. degree in internal geophysics and Ph.D. degree in seismology from the Université Paris VII - Institut de Physique du Globe de Paris, Paris, France, in 1998 and 2002, respectively.

After a Postdoctoral Fellowship with the Department of Earth Sciences, University of Oxford, he was hired as an Assistant Professor with the Laboratory of Planetology and Geodynamics, University of Nantes, in 2004. He became a Full Professor in 2018. His past and present researches concern global and regional seismology. He is deeply involved in the construction of the French permanent broadband seismic array. He has developed nonlinear inverse procedures to infer the interior of planets and to detect and locate small magnitude seismic sources. He is the Co-I of the instrument SEIS (InSight NASA mission).



E. Diego Mercerat received the M.S. degree in applied geophysics from ITC, Delft, The Netherlands, in 2001, and the Ph.D. degree in civil engineering and geomechanics from the National Polytechnical Institute of Lorraine, Nancy, France, in 2007.

He then served as a Postdoctoral Fellow with the Institut de Physique du Globe de Paris and with the University of Nice Sophia-Antipolis, Nice, France, working on seismic modeling and tomography. Since 2011, he has been a Researcher in seismology working for the French Ministry of Ecology, Sustainable Development and Energy, with joint appointments at CEREMA Méditerranée and at the Géoazur Laboratory, University of Côte d'Azur, Sophia-Antipolis, France. His research interests include seismic wave modeling and inversion, seismic response of civil engineering structures and geomorphological features, and seismic hazard assessment.

Dr. Mercerat is a member of the Scientific Committee of the RAP-RESIF consortium (French Accelerometric Network).



David Ambrois received the M.S. degree in marine geophysics from the European Institute of Marine Sciences, Brest, France, in 2013.

Since 2013, he has been an Engineer with the Géoazur Laboratory, Sophia-Antipolis, France. He specializes in seismological data processing. He was in charge of improving the automatic earthquake detection system in the South East of France. He has participated in numerous research projects, in particular on seismicity in Ecuador and more recently on Marsian seismicity.



Romain Schwab received the M.S. degree in hydrography from École Nationale Supérieure des Techniques Avancées de Bretagne (ENSTA Bretagne), Brest, France, in 2015.

From 2015 to 2018, he was a Research Engineer on the detection and localization of buried targets in marine environment within a project funded by the French Ministry of the Armed Forces. Since 2019, besides his research work, he has been in charge of the sensors (multibeam echosounder, single-beam echosounder, sidescan, acoustic Doppler current profilers, etc.) and experiments at ENSTA Bretagne. He is a member of the Association Francophone d'Hydrographie and the Head of its Technical Group.



Paul Cristini (Member, IEEE) graduated from École Nationale Supérieure de Physique de Marseille, Marseille, France, in 1986, and received the M.S. degree in acoustics and Ph.D. degree in acoustics from the University of Aix-Marseille II, Marseille, France, in 1988 and 1991, respectively.

Since 1991, he has been a Researcher with the French National Centre for Scientific Research, France. From 1991 to 2000, and then from 2000 to 2008, he was successively with the Laboratory of Mechanics and Acoustics (LMA), Marseille, France, and with the Laboratory of Modeling and Imaging in Geosciences, Pau, France, respectively. Since 2008, he has been with the LMA working on numerical modeling of wave propagation in underwater acoustics for various applications with emphasis on the use of high-performance computing.

Dr. Cristini is a member of the Acoustical Society of America and of the French Society of Acoustics.



Fang Wang graduated from École Centrale de Marseille, Marseille, France, in 2012, and the Ph.D. degree in geophysics from Mines ParisTech, Paris, France, in 2016.

Her thesis work concerned waveform inversion. From 2017 to 2019, she was a Postdoctoral Fellow with the Laboratory of Mechanics and Acoustics, Marseille, France, working on numerical simulation of seismo-acoustic wave propagation. Since 2020, she has been a Geophysicist for Compagnie Générale de Géophysique, Massy, France, currently working on land seismic imaging projects.